Public domain. CC0 1.0.





# Beyond the 100-Year Flood: Probabilistic Flood Hazard Assessment for King and Pierce Counties under Future Climate Scenarios

Kees Nederhoff<sup>1</sup>, Kai Parker<sup>2</sup>, Eric Grossman<sup>2</sup>

- <sup>1</sup> Deltares USA, 8601 Georgia Ave, Silver Spring, MD 20910, USA
- 5 <sup>2</sup> U.S. Geological Survey, Pacific Coastal and Marine Science Center, Santa Cruz, CA 95060, USA

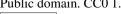
Correspondence to: Kees Nederhoff (kees.nederhoff@deltares-usa.us)

Abstract. Coastal areas, such as the Salish Sea, are becoming increasingly vulnerable to compound flooding due to the 10 interaction between storm surge, tides, and river outflow. This hazard is anticipated to increase under sealevel rise and climate change. This research offers a high-resolution flood hazard mapping for King and Pierce Counties of Washington State (United States of America) using the SFINCS (Super-Fast INundation of CoastS) model to facilitate a Continuous Flood Response Modeling (CFRM) framework wherein decades of dynamic coastal and fluvial processes are simulated. By applying a cellby-cell extreme value analysis, we predict flood areas for return periods of 1-100 years and compute the Expected Annual 15 Flooded Area (EAFA) as a probability-weighted indicator of flood exposure. Model validation against National Oceanic and Atmospheric Administration (NOAA) and United States Geological Survey (USGS) gauge data demonstrates skill (RMSE: 14-17 cm for coastal water levels; unbiased RMSE: 49-116 cm for river water levels), and comparison with FEMA Special Flood Hazard Areas shows high spatial agreement of flooding (hit rates: 0.75-0.83). The timing statistics of the flooding reveal that the December 28, 2022, event was responsible for most historically observed flooding across the area. Climate simulations for today show EAFA ranges from 56 to 200 hectares in King County and from 250 to 644 hectares in Pierce County. Future projections show that sea level rise is the main contributor to increasing flood extent, whereas climate change drivers such as storm pattern change have little additional effect. We also identified a threshold around 100-150 cm of sea level rise at which the flood-exposed area increases substantially. Additionally, simplified deterministic flood maps can underestimate flood hazard by up to 0.5 m if not all relevant drivers are included. These results support the use of probabilistic, event-independent flood metrics such as EAFA to inform more rational and spatially responsive flood risk management.

# 1 Introduction

Coastal and estuarine communities face increasing vulnerability to flooding due to the combined effects of sealevel rise (SLR), storm surges, high tides, and fluvial discharge. Globally, over 600 million people live within 10 m of sea level, a number projected to exceed 1 billion by 2050, and accelerating SLR could displace many and incur trillions of dollars in annual flood damages by the end of the century (Barnard et al., 2019). In the Pacific Northwest (PNW) of the United States, including the Puget Sound region of King and Pierce Counties (Washington State, United States of America), this threat is acute with important implications for these two most populous counties in Washington State and the Ports of Seattle and Tacoma (Miller et al., 2023). King and Pierce Counties border the Salish Sea, a large, transboundary estuarine system including Puget Sound,

Public domain. CC0 1.0.





PUBLIC DOMAIN

the Strait of Juan de Fuca, and the Strait of Georgia, with complex bathymetry, strong tides, and variable meteorological 35 forcing (Grossman et al., 2023). Anticipated future rise in mean sea level and intensification of winter storms (Tohver et al., 2014) will likely increase coastal flood hazards (Ruggiero, 2013). When SLR along the shoreline (from tides and surges) combines with high river discharge, the resultant compound flooding is far more devastating compared to flooding by any single driver alone (Wahl et al., 2015). Recent research reveals that most flood events at most U.S. coastlines involve more than one driver happening simultaneously, and compound events carry a disproportionate share of flood damages (Ali et al., 2025). An increase in the rate of urban development and loss of natural flood buffers in flood-prone coastal plains increases still further the flood risk of towns, amplifying the urgency for managing these risks under climate change (Wing et al., 2022).

Effectively managing compound flood hazards is challenging because most traditional flood assessments do not capture the joint and temporally variable nature of these events. Common practice in the majority of engineering studies and flood mapping 45 efforts is to use single-event (deterministic) scenarios (e.g., the '100-year' design storm), treating flood drivers in isolation (Green et al., 2025). While this event-based method is straightforward and widespread, it misrepresents the flood risk since such methods fail to consider the chances of multiple extremes blending into a single event or co-occurring. For instance, "design floods" are often unable to account for the time difference between different physical drivers, such as the moment of the tide, storm surge peak, or river flood wave. As a result, such deterministic scenarios fail to incorporate compounding effects and mischaracterize flood hazard. This limitation is particularly significant in the Salish Sea, where high water levels are tightly controlled by interactions of tides, storm surges, and freshwater runoff.

Earlier studies, such as those of Yang et al. (2020) and Soontiens et al. (2016), have modeled 34 and 5 extreme events, respectively, based on event-based models in efforts to model surge dynamics. The earlier studies, though, involved preselecting certain storms to model, which was limited by the area's high tidal range. For instance, Abeysirigunawardena et al. (2011) indicated that 5% of the maximum surges in Canadian waters of the Salish Sea occurred at high tide. This is an indication of how important it is to represent tidal amplitudes and phasing, surges, timing, and compound tide-surge interactions in representing the overall description of flood risk. Furthermore, the intricate system of estuaries, basins, and channels that constitute the Salish Sea results in significant spatial heterogeneity in the behavior of local water levels under 60 forcing from storms. For these reasons, selecting a few events may not be sufficient to represent the complete spatial variety of possible flood effects across the region.

To better capture these complexities, the scientific and engineering community has increasingly shifted from deterministic toward probabilistic frameworks. For example, copula techniques are now widely used to preserve interdependence among variables (for example, wave height and period, but also storm surge and river discharge) in the event generation process (e.g., Couasnon et al., 2020). A well-established example in this direction for tropical cyclones is the Joint Probability Method (JPM), which synthetically creates many storm scenarios with different landfall locations, intensities, and angles to acquire

Public domain. CC0 1.0.



70

95



flood frequency estimates (Resio and Irish, 2015). These probabilistic forcing-based methods provide more robust estimates of hazards than single-event methods by integrating across the full variability of driver combinations.

From this foundation, response-based evaluations of flood hazards take the next step by dynamically simulating the flooding for an extensive set of synthetic events, and subsequently empirically determining flood probabilities from simulated outcomes (Gori et al., 2020). Flood probabilities are calculated at each location in the area of interest, and no assumption of "extremeness" for events is used. Rather, this method allows the system response to determine risk rather than inferring risk from statistics of driver attributes alone. Advances in computation in recent years and cost-effective hydrodynamic solvers have rendered such ensemble simulations more viable. For example, Santamaria-Aguilar et al. (2025) performed over 5,000 compound flood simulations with an SFINCS implementation on the graphics processing unit (GPU), producing probabilistic flood maps that account for both temporal and spatial uncertainty. Similarly, Nederhoff et al. (2024) utilized a response-based probabilistic method for compound flood risk assessment along the southeast coast of the U.S. for both tropical and extratropical events. One of the benefits of this approach is the inclusion of low-probability but high-consequence scenarios (e.g., a 10,000-year cyclone landfall). Rare events can thus be integrated with frequent ones into a single modeling framework that consistently evaluates their contribution to flooding hazard and risk.

Parallel to these developments, continuous simulation (CS) approaches have emerged as an alternative to event-based flood estimation, offering closer links to physical processes and avoiding assumptions about conditions (Viviroli et al., 2022). A natural evolution is to combine response-based compound flood modeling with continuous simulation in what we term Continuous Flood Response Modeling (CFRM). CFRM applies decades-long, continuous boundary forcing and includes tides, surge, and river discharge to coupled hydrologic—hydrodynamic models. This approach eliminates the need to pre-select design events or construct synthetic joint probability scenarios. Unlike traditional approaches, CFRM captures the co-occurrence, sequencing, and persistence of flood drivers physically and temporally, without relying on predefined storm hydrographs (Dent et al., 2011). Continuous simulation has been used extensively in riverine flood studies but has rarely been applied to compound coastal and estuarine flooding due to computational demands. CFRM may thus represent one of the first implementations of a fully continuous, decades-long simulation approach specifically for compound flood hazard assessment in a complex estuarine setting.

Building on these principles, we develop and apply a CFRM framework for compound flood hazard assessment in King and

Pierce Counties, Washington. Our approach uses the Super-Fast INundation of CoastS (SFINCS) model (Leijnse et al., 2021) and uses its computational efficiency to simulate continuous water levels and flows under decades of climate variability. This implementation is based on the Coastal Storm Modeling System (CoSMoS), a widely used modeling framework first developed for California (Barnard et al., 2019; O'Neill et al., 2018). Our study extends the Puget Sound implementation (PS-CoSMoS) of Nederhoff et al. (2024), which developed regional-scale storm hazard projections for Whatcom County, by

Public domain. CC0 1.0.



105

110

120



improving the representation of coastal—riverine interactions and porting the approach to a new geography. Specifically, we focus on overland flood dynamics in King and Pierce Counties and demonstrate how such a method can be used in other sheltered estuarine habitats around the world. Using SFINCS, we simulate continuous water levels and flows across the study area under decades of climate variability, allowing every grid cell to experience the full range of tide, surge, and river discharge combinations over the multi-decade period. This enables a cell-specific extreme value analysis, wherein flood frequency statistics (e.g., 100-year water levels) are derived at each model grid cell from the long-term simulation output, rather than being assumed from a single event. The modeling system is first validated against observed water levels and flood extents to ensure credible performance. We then apply the validated model to quantify both current and future flood hazards under various SLR and climate change scenarios. This CFRM approach offers a novel, probabilistic view of compound flooding for the Salish Sea region.

## 2 Study site: King and Pierce County

Spanning British Columbia, Canada, and Washington State, USA, the Salish Sea is a complex estuarine system formed from flooded glacial valleys, including the Strait of Georgia, Puget Sound, and the Strait of Juan de Fuca. The unique arrangement of channels, islands, and shoals is fed by numerous freshwater watersheds. Ocean waves reach this basin through the constricted route of the Strait of Juan de Fuca, and local winds determine the wave climate elsewhere in other fetch-limited regions (Grossman et al., 2023). The meandering and irregular shoreline of the Salish Sea demonstrates the dynamic and geographically variable setting. It also adds highly exceptional marine biodiversity and benefits the economy and culture of a prosperous and growing coastal community in cities such as Seattle and Tacoma, Washington, and Vancouver, British Columbia (Oldford et al. 2025).

King and Pierce Counties lie within the central Puget Sound region of Washington, which is bound on the west by the Salish Sea and Kitsap County, on the north by Snohomish County, and on the south by Thurston & Lewis Counties (Figure 1). The counties cover more than 10,000 km² of heterogeneous geology and ecosystems from coastal estuaries to glaciated volcanic peaks. King County, where the largest city, Seattle, is located, and Pierce County, where the largest city, Tacoma, is situated, have large populations and are economic centers. Both possess high-density populations, urbanized infrastructure, and economically valuable resources in the coastal zone and would benefit from accurate risk assessments, allowing shoreline planners to better manage the combined impacts of SLR and extreme events. Land use ranges from heavily developed urban zones to productive agricultural lands, particularly in the lowland deltas and tidal flats that are vulnerable to erosion and flooding (Grossman et al., 2023).

Topographically, the county terrain ranges from sea level to over 4,300 meters at the summit of Mount Rainier, an active volcano and the state's highest point. Mount Rainier provides sustenance for numerous streams and glaciers that produce

Public domain. CC0 1.0.





river systems of steep gradient and high velocity, carrying water and sediment from alpine to marine environments (Sisson et al., 2001). The largest rivers in the area, such as the Duwamish and Green Rivers in King County and the Puyallup River in Pierce County drain large watersheds that include agricultural fields and urban areas before emptying into Puget Sound. These rivers yield to Puget Sound lowlands and form broad estuaries and deltas at their mouths that support an array of nearshore and tidal marsh communities. Geological data show that in the past, volcanic lahars from Mount Rainier have blanketed the Puyallup Valley, highlighting the connection between mountain and coastal floodplains (Sisson et al., 2001).

Other important features include Vashon Island within King County, located in the middle of Puget Sound, and parts of the Kitsap Peninsula in Pierce County. Both geographic features contribute to local coastal processes and ecosystems. Long stretches of the shore have eroding bluffs, mixed-sediment beaches, tidal flats, and man-made shoreline structures like seawalls. These structures reduce natural wave dissipation and increase direct wave impacts at high tide. Nearly a third of Puget Sound's ~4,000 km of shore is armored, often producing steeper, finer beaches, reduced habitat, and perturbed sediment transport (Dethier et al., 2016).

The Salish Sea tides consist of a mixed semi-diurnal meso-tidal regime, where tidal amplitudes are amplified as they enter the system from the Pacific Ocean. Tidal amplitudes increase from about 2.4 m at the ocean mouth to 4.4 m farther inland (e.g., Olympia, Washington), with strong currents (often >1 m/s) through restricted passages like Admiralty Inlet (Grossman et al., 2023). Storm surges are predominantly a result of severe low-pressure weather systems forming over the eastern Pacific Ocean that travel onshore between Oregon, USA, and Vancouver Island, British Columbia (Yang et al., 2019). High coastal water levels in the Salish Sea are therefore a result of a combination of offshore (Pacific Ocean) steric sea-level anomalies (remote SLA), inverse barometer effect, and setup by wind. Maximum surge amplitudes will usually be of up to ~1 meter (e.g., Grossman et al., 2023). Wave climate in the Salish Sea is complex; the outer coast and western Strait of Juan de Fuca are dominated by swell and have wave periods normally >10 s, while Puget Sound is dominated by wind-sea with wave periods normally <5 s and wave heights <2 m (Crosby et al., 2023).

There are some recent and historic flood events that have demonstrated the vulnerability of the region to both coastal and fluvial flooding. For instance, on 28 December 2022, a flooding event resulted in widespread inundation in Seattle's South Park neighborhood (Thomas, 2023). Commonly referred to as a 'King Tide' event, it was 3.8 m+ the North American Vertical Datum of 1988 (NAVD88) above NOAA Seattle tide gauge (#9447130) and had significant impacts in low-lying urban areas aggravated by pre-spring snowmelt, a low-pressure system, and stormwater runoff. Among some of the other important incidents are the flood in December 1975 that affected the Nisqually and Green Rivers (U.S. Army Corps of Engineers, 1977) and the November 1990 flood, when storms during Thanksgiving week caused general riverine flooding throughout the whole Pierce County (Hubbard, 1993). These events, both in urban and rural areas, emphasize the importance of coupled flood modeling and planning initiatives able to capture the spatial and temporal heterogeneity of compound flood risk across the Puget Sound region.





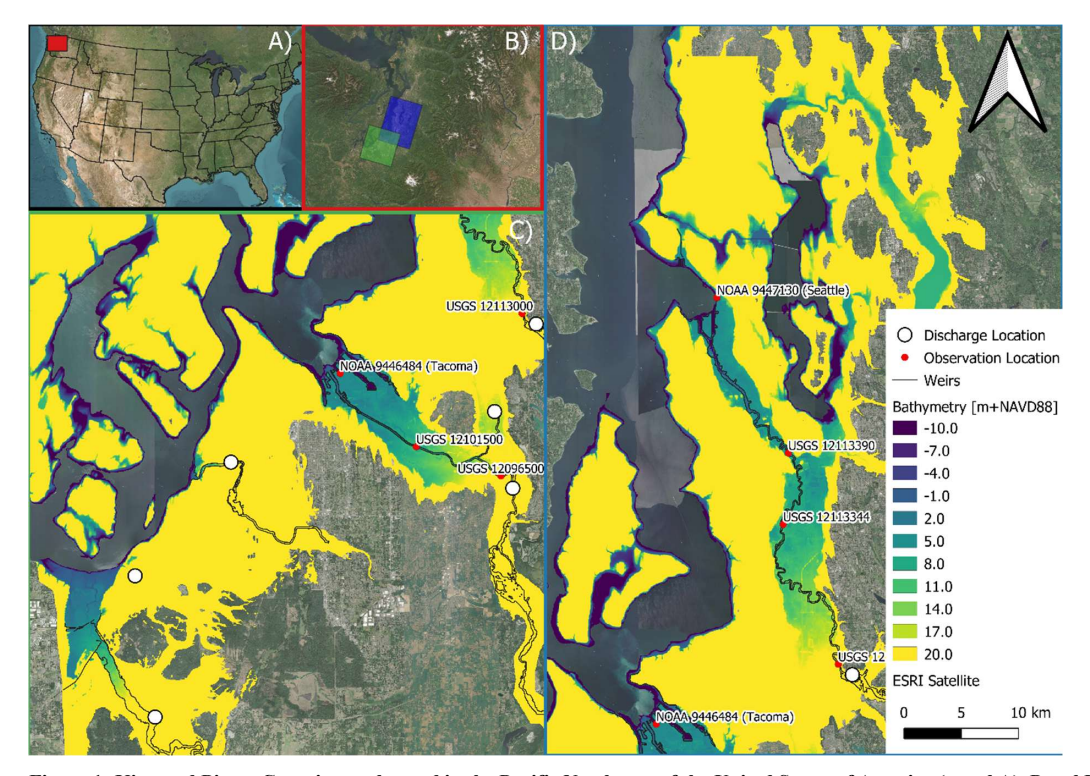


Figure 1: King and Pierce Counties are located in the Pacific Northwest of the United States of America (panel A). Panel B provides an overview of the area of interest in King County (blue domain) and Pierce County (green domain), Washington, and the SFINCS model domains. Panel C provides a detailed view of Pierce County and Panel D provides a detailed overview of King County. Note that there are five inflow boundary conditions in total, but due to partial overlap between panels C and D, some boundaries appear duplicated. Two NOAA stations are included 944713 (Seattle) and 9446484 (Tacoma) and 5 USGS stations (12096500, 12101500, 12113000, 12113344, 12113390) – see NOAA (2025) and U.S. Geological Survey (2025) for more information. Background: Esri World Imagery basemap. Sources: Esri, Maxar, GeoEye, i-cubed, USDA FSA, USGS, AEX, Getmapping, Aerogrid, IGN, IGP, swisstopo, and the GIS User Community.

## 3 Materials and methods

## 3.1 Overview

This study's modeling approach builds on CoSMoS (Barnard et al., 2014), originally developed for California and later adapted for Washington State (Crosby et al., 2023; Grossman et al., 2023; Nederhoff et al., 2024). Figure 2 displays the conceptual framework as applied here. Overland flooding was simulated using the open-source model SFINCS (Leijnse et al., 2021), which was selected for its computational efficiency and ability to represent dynamic flood processes. Two high-resolution model domains were constructed for King and Pierce Counties incorporating high-resolution topobathymetric data and land cover (Section 3.2.1). Boundary conditions for water levels and river discharges were provided from multi-century



climatological datasets (Section 3.2.2). The modeling was conducted in two phases: first, the reanalysis period was simulated and validated against observational datasets (Section 4.1). Second, future climate conditions were simulated under multiple SLR scenarios. Compound flood outputs from these simulations and extreme value analysis were used to estimate flood frequency and were subsequently downscaled to higher spatial resolution (Section 4.2). The following sections describe the input data, model components, numerical methods, and computational framework in greater detail.

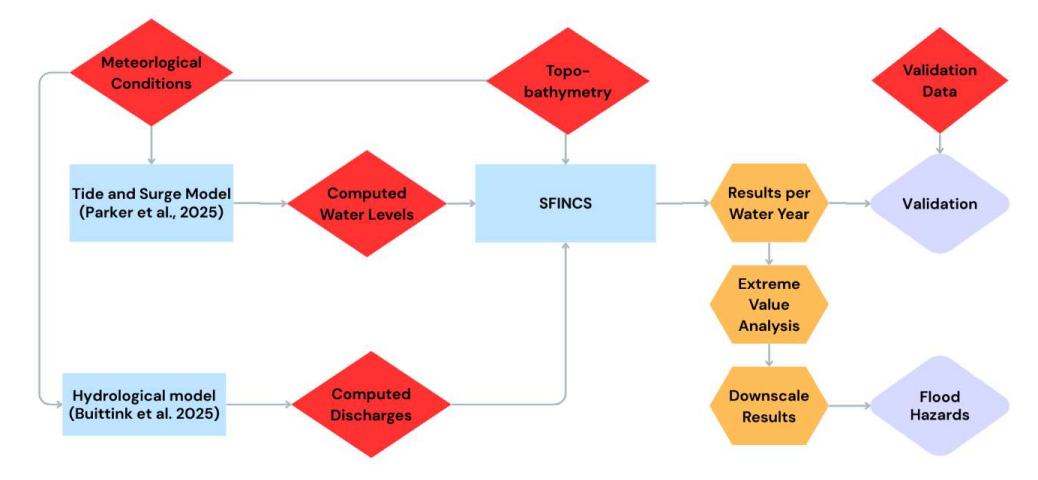


Figure 2. Conceptual workflow of the CoSMoS flood modeling framework. Blue rectangles represent model components, red diamonds indicate input data sources, orange hexagons denote analysis steps, and purple rounded diamonds show the main outputs of the study.

## 3.2 Input data

190

200

205

#### 195 3.2.1 Static data: topobathymetry and land roughness

Elevation data for the entirety of the coastal regions of King and Pierce Counties were derived from the Coastal National Elevation Database (CoNED) topographic model of Puget Sound (Tyler et al., 2020). The CoNED dataset provides a seamless digital elevation model (DEM) at 1-meter resolution, constructed from the latest high-resolution datasets, including light detection and ranging (LiDAR) topography, multibeam and single-beam bathymetry, and other topographic and bathymetric sources. These datasets were merged into a continuous surface to ensure spatial consistency and accuracy. For this study, CoNED data were extracted to create DEMs necessary for running the SFINCS model. The CoNED DEM has a root-mean-square error (RMSE) of 22 cm, which reflects its reliability for this type of coastal hazard analysis.

The subsampled CoNED DEMs were used to characterize the nearshore zone, beach areas, riverine channels, and levees as accurately as possible. Elevation data are the first-order control on flood hazard modelling fidelity, and a high resolution and level of detail are critical for capturing the hydrodynamic processes that govern coastal and riverine flooding. Early model

Public domain. CC0 1.0.



210



runs, however, revealed inaccuracies in the representation of riverine bathymetry. To address this, additional data were utilized to infer riverine bathymetry characteristics for the major river systems. Modified riverine bathymetry was found to improve the representation of channel morphology and flow dynamics within the SFINCS simulations. In particular, a trapezoidal channel shape was imposed along the Green and Puyallup Rivers to replace the hydro-flattened bathymetry, which was too shallow. The channel centerlines were defined by digitizing a line along the thalweg, and cross-sections were deepened to a trapezoidal profile to improve hydraulic connectivity in the model.

The National Land Cover Database (NLCD; Homer et al., 2020) was utilized to define spatially variable roughness over the SFINCS model domain. Comparable translations, as in Nederhoff et al. (2021), were used to convert land cover classes into friction values. This approach enabled the representation of heterogeneous surface characteristics, with roughness values ranging from 0.020 for open water to 0.15 for forests. Open water friction was set to a constant 0.020 value and was thus not used for calibration. This spatially variable roughness enhances the model's ability to simulate flood behavior across a variety of land cover and hydrologic regimes.

## 220 3.2.2 Dynamic forcing conditions: water levels and discharges

Water levels and wave heights were extracted from regional Delft3D FM and SWAN modeling efforts (Parker et al., in preparation). Specifically, a Delft3D Flexible Mesh (Delft3D FM) model was used to compute tides and surges across the Salish Sea. The model exhibited high skill in replicating still water levels compared to six National Oceanic and Atmospheric Administration (NOAA) tide stations and seven U.S. Geological Survey (USGS) tide gauges across the 2017-2019 validation period (Figure 1), with a mean error of approximately 10 cm (Grossman et al., 2023). Still water levels (water levels driven by tides, steric sea-level anomalies, and storm surges) were directly extracted from the regional Delft3D FM model and imposed as time-varying water level boundary conditions along the open coast of our SFINCS domains. Waves were computed as a sum of locally generated wind waves and the linear transformation of the Pacific Ocean swell. This approach enables quick wave predictions at high spatial resolution, making long-term regional simulations possible, with skills similar to standard SWAN implementations (Crosby et al., 2023). Wave height was converted into wave setup through the 20% of the wave height approximation commonly used in coastal engineering (e.g., Vousdoukas et al., 2018) and added to the still water levels computed by the Delft3D model. This simplified approach was chosen for efficiency but could misrepresent run-up in some locations.

Stream inflow discharges were simulated using the wflow hydrological modeling framework (van Verseveld et al., 2024). The wflow model allows for the simulation of key catchment hydrological processes, including precipitation, interception, snow accumulation and melt, evapotranspiration, soil water, surface water, and groundwater recharge, within a fully distributed environment. Discharges were imposed at five locations (1 in King County and 4 in Pierce County), at approximately +20 m NAVD88, which is considered outside the zone of tidal influence (Figure 1 – black circles with white fill). Discharges were

https://doi.org/10.5194/egusphere-2025-4909

Preprint. Discussion started: 11 November 2025

Public domain. CC0 1.0.





typically within a 20% error margin of observed flows, based on the calibration/validation of the wflow model in the region (Buitink et al., 2025). For more information on this regional modeling work, one is referred to Buitink et al. (2025).

All model domains were forced using meteorological conditions, including wind speed and mean sea-level pressure. These meteorological inputs were applied in the upstream/regional models (e.g., atmospheric forcing for Delft3D FM and wflow), ensuring that storm effects were represented in the boundary water levels and river inflows passed to SFINCS. No direct wind or rain forcing was applied within the SFINCS domains. For the hindcast (validation) period from 1941 to 2022, meteorological inputs were based on ERA5 reanalysis data (Hersbach et al., 2020). For the projection period, conditions were derived from the Coupled Model Intercomparison Project - Phase 6 (CMIP6). An ensemble of 7 CMIP6 models from the High-Resolution Model Intercomparison Project (HighResMIP, Haarsma et al., 2016) was used with the SSP5-8.5 greenhouse gas concentration scenario. Models from the HighResMIP project were selected for their higher spatial resolution (25–50 km), which is expected to improve the representation of coastal storm events that are inadequately resolved by the native resolution of most general circulation models (GCMs; Roberts et al., 2020). As a compromise for higher resolution, models in the HighResMIP project were run for a shorter simulation time (1950-2050) than other CMIP6 models. Therefore, conclusions regarding temporal changes in forcing are limited to this time horizon. More details on the specific CMIP6 model iterations used and their implementation in the regional framework can be found in Parker et al. (in preparation).

To assess the impact of SLR on flooding in King and Pierce Counties, seven SLR scenarios were selected: 0, 0.25, 0.50, 1.00, 1.50, 2.00, and 3.00 meters above mean sea level in the year 2005. These scenarios were selected to bracket the potential magnitudes of SLR without consideration of particular time frames so that flexibility is provided for future re-analysis as relative SLR projections are refined. This response aligns with the suite of SLR projections for the U.S. West Coast through the year 2100 presented by Sweet et al. (2022) and previous CoSMoS modeling research (Barnard et al., 2014).

#### 3.3 Validation data

260

#### 3.3.1 Coastal water levels: NOAA

Time series of observed water levels at NOAA stations (Figure 1 – red circles with prefix "NOAA" labeling) across the study area were utilized to validate the model. Hourly water levels relative to NAVD88 were obtained from two NOAA stations for the period 1942–2022. The Seattle, WA station (Station ID: 9447130) has a continuous record, while the Tacoma, WA station (Station ID: 9446484) started operating in 1996 (NOAA, 2025).

## 3.3.2 Riverine water levels USGS

Streamgage time series of observed water levels from USGS (Figure 1 – red circles with "USGS" prefix labeling) were used to validate the inland conditions model. River stage data from 2007 to 2022 were collected at five USGS stations. Because the

Public domain. CC0 1.0.



280

285



reference level of stage measurements can be non-uniform, all the comparisons were adjusted to make a fair comparison between the model (referenced to NAVD88) and the USGS observed gage heights.

# 3.3.3 Flood extent: FEMA maps

Federal Emergency Management Agency (FEMA) Special Flood Hazard Areas (SFHAs) were used as reference data to validate modeled flood extents. SFHAs illustrate zones of a 1% annual chance of flooding (commonly referred to as the "100-year floodplain") and are the primary regulatory flood zones mapped in FEMA's Flood Insurance Program. These zones are established through site-specific analysis that commonly involves hydrologic and hydraulic modeling, which may vary from simplifying assumptions to complex 1D or 2D simulations depending on local conditions and data availability. In this study, FEMA-provided vector shapefiles of the 1% Annual Exceedance Probability (AEP) floodplain were used for comparison with simulated flood extents (Federal Emergency Management Agency, 2025). However, there are no detailed metadata available to describe the underlying data, making it nearly impossible to determine the data's age, resolution, or methodology for each jurisdiction. To allow for pixel-based validation, all FEMA shapefiles were rasterized to a 2-meter resolution grid and reclassified into three classes: flooded (wet), not flooded (dry), and no data. These raster FEMA maps enabled pixel-by-pixel comparison to modeled flood extents, from which we computed categorical skill metrics (hit rates, false alarm ratios, etc.) described in Section 3.3.

#### 3.4 Numerical method: overland flooding with SFINCS

SFINCS (Leijnse et al., 2021; van Ormondt et al., 2024) was used to simulate compound flooding processes, encompassing dynamic hydraulic phenomena such as tidal propagation and river runoff while ensuring computational efficiency (e.g., Sebastian et al., 2021). This combination of capabilities made SFINCS an ideal choice for predicting overland flooding in this study. Two computational domains were developed for King and Pierce Counties (refer to Figure 1 – panels C and D), each constructed at a 50-meter resolution, covering an average area of 3000 km². These domains incorporated 1-meter resolution CoNED topobathymetric via subgrid tables (which store the elevation at 20 vertical levels) to preserve fine-scale topography within each 50 m cell. All simulations were conducted with advection enabled, turning SFINCS into a solver for the Simplified Shallow Water Equations (SSWE).

295

300

No calibration of the SFINCS computations was performed, as simulated regional water levels and riverine inflow discharges were directly imposed, and friction in open water was held constant. Overland flooding was allowed to infiltrate at a constant 2 mm/hr (representing low-permeability soils Rawls et al., 1982), to provide a rudimentary representation of drainage and prevent indefinite ponding in flat areas. Rainfall or wind forcing were not directly applied in the model, but these factors were used to derive regional boundary conditions for water levels and discharges.

https://doi.org/10.5194/egusphere-2025-4909

Preprint. Discussion started: 11 November 2025

Public domain. CC0 1.0.



305

310



Simulations were conducted for complete water years (WY; a 12-month period from October 1 through the following September 30 and named for the year in which it ends), precdeded by a 7-day initialization period (spin-up period). Key outputs recorded during the simulations included the maximum annual water level, the maximum depth-velocity product (m²/s), the duration that each cell remained wet using a minimum depth of 10 cm, and the time of maximum water level.

The model results were generated using a slightly modified version of the SFINCS "Dollerup" release from November 2023, which is available as open-source code on GitHub and through Deltares (van Ormondt et al., 2025; <a href="https://github.com/Deltares/SFINCS">https://github.com/Deltares/SFINCS</a>; available from September 1, 2025 on GitHub). In particular, we added new output functionality that tracks the moment of high water. These changes have recently been merged into the main trunk of the code on GitHub.

To account for uncertainty in boundary conditions, an additional two simulations were performed with altered "low" and "high" estimates of parameters. The low estimate reduced dynamic coastal water levels by 50 cm, lowered river discharge by 20%, and increased weir crest elevations by 50 cm to represent a more conservative (lower hazard) scenario. Conversely, for the high estimate, the same parameters were adjusted but in the opposite direction to simulate a more demanding (higher hazard) boundary condition. These are constructed to simulate a 95% confidence interval, based on normally distributed model residuals and ±2 times the root-mean-square error (RMSE) enclosing the likely range of flood response. This allows us to examine the sensitivity of predictions of flood extent to uncertainty in the dominant (hydrodynamic) inputs. Results from these High/Low hazard simulations are used later to define uncertainty ranges.

## 3.5 Computational framework, simulation period, and computational expense

The modeling framework was structured into three distinct phases: (1) reanalysis (hindcast) validation, (2) current climate projections, and (3) future climate projections.

- During the validation phase, the model was validated over an 82-year reanalysis period spanning water years 1941 through 2022. Coastal water levels were validated using observations from two NOAA tide gauge stations (Seattle and Tacoma, WA), while inland water levels were assessed using data from five USGS streamgages distributed across King and Pierce Counties (Figure 1).
- 330 To support extreme value analysis, the model was driven with 82 years of reanalysis boundary conditions (1941–2022), enhanced by applying randomized tidal phasing. This approach generated an additional 18 synthetic years, bringing the total timeseries to 100 years, ensuring adequate sampling of extreme events. Importantly, this method enabled an empirical estimation of 100-year return levels, avoiding the need to fit a theoretical extreme value distribution. In particular, the method from Nederhoff et al. (2024) for a synthetic record was utilized by randomly selecting a yearly non-tidal-residual (NTR) signal

Public domain. CC0 1.0.





from the 82-year record. NTR refers to all non-tidal fluctuations in sea level and includes, for example, contributions from steric sea level anomalies and wind-driven storm surge. A uniform distribution shift from -1 to +1 days was applied to the time axis of the NTR to increase variability. Tides were generated from astronomical components computed from the tide-only regional model results. Discharge and wave conditions were assumed to be completely correlated with NTR, and associated wind and wave conditions are directly used in model forcing.

340

350

355

In the future climate phase, the model was forced using the pseudo-global-warming (PGW) approach (Brogli et al. 2023). The PGW strategy consists of simulating the current conditions with boundary conditions modified by the climate change signal (delta). In this case, the same reanalysis 100-year simulation was re-run with all boundary conditions (water levels and riverine discharges) modified by a calculated climate change signal. The utilized delta was calculated by running the regional models (both water level and streamflow), forced by an ensemble of CMIP6 models. The CMIP6 forced ensemble was run for both a historical and future period, with the change (the delta in the PGW method) then calculated at all boundary forcing points used in this study. The delta was calculated by computing the difference between the future and historical cumulative distribution function (CDF) at all quantiles in the CDF, allowing a variable delta across the CDF. This approach allows flexibility in how water levels might change, for example, extremes increasing while the average water level stays the same. In essence, this applies a quantile-dependent shift to every time step of the historical boundary conditions so that their statistical distribution matches that projected for mid-century climate. To allow for seasonal differences in the climate change signal, this delta was calculated for each month of the year. The full ensemble of calculated deltas (7 climate models, 12 months, all quantiles) was reduced by taking the average across the CMIP6 ensemble members, with averaging used to reduce individual CMIP6 bias and improve robustness of the resulting calculated delta signal. This delta was then applied to the full timeseries of the current climate projections period to produce a new boundary forcing PGW timeseries representing the future period. Simulations using this PGW future climate were then conducted for multiple SLR scenarios to evaluate the sensitivity of flood hazards to different future climate trajectories. In this way, future changes to flood hazards are segmented into 2 signals: a climate change forcing signal (provided using the PGW method), and an SLR signal (implemented as a change to Mean Sea Level).

360 Flood hazards are often defined by wet areas based on a specific flood depth threshold, typically 10 or 15 cm (e.g., Wing et al., 2017). In this paper, we apply three classes of flood severity: nuisance flooding (depth > 10 cm), hazardous flooding (depth > 30 cm), and severe flooding (depth > 100 cm). The flood hazards were analysed over a full range of return periods from 1 to 100 years. We also computed the Expected Annual Flooded Area (EAFA), as a probability-weighted sum of flood extents for all return periods, and computed this for each severity class separately (Vousdoukas et al., 2023). To focus on event-driven flooding, grid cells that flood during regular daily tidal conditions were not included in these calculations.

All the simulations were executed on the USGS Hovenweep platform (Falgout et al., 2025). A single simulation run (one water year) required approximately 36 hours to finish. We simulated the current climate scenario at mean sea level (0 m SLR) and

Preprint. Discussion started: 11 November 2025

Public domain. CC0 1.0.





at one elevated SLR level (1.0 m) to isolate SLR-only effects. Under future climate (PGW conditions), we ran the full set of seven SLR scenarios (0 through 3 m). In total, 5,400 yearly simulations (7x SLR scenarios with future climate and 2x SLR for current climate, 3 uncertainty layers, and 2 domains) were conducted, totaling a computational effort of approximately 194,400 hours. However, the actual computational burden was an order of magnitude higher due to additional sensitivity tests, calibration runs, and model refinements in an iterative stakeholder process. In order to quantify uncertainty in SLR projections, each scenario was rerun with both high and low estimates, totalling 2700 simulations. This extensive simulation effort offers robust statistical analysis, multiple scenarios to address the requirements of stakeholders, and testing to address both past and future flood conditions.

#### 3.6 Model skill

To quantify the skill of the model to reproduce water levels, several accuracy metrics were calculated: model bias, mean-absolute-error (MAE; Equation 1), root-mean-square-error (RMSE; Equation 2), and unbiased RMSE (uRMSE; RMSE with bias removed from the predicted value)

$$MAE = \frac{1}{N} \sum (|y_i - x_i|)$$

Equation 1

$$RMSE = \sqrt{\frac{1}{N}\sum (y_i - x_i)^2}$$

Equation 2

where N is the number of data points,  $y_i$  is the i-th predicted (modeled) value, and  $x_i$  is the i-th measurement. For stations without a reference level, we computed the unbiased RMSE and MAE, also referred to as uRSME and uMAE. Lastly, we compute the scatter index (SCI), which is a metric to express RMSE in a relative sense as a fraction of the RMS magnitude of the signal.

385

390

380

In addition to these continuous metrics, a binary skill classification was used to evaluate the model's ability to correctly predict wet and dry conditions (Wing et al., 2017). For this classification, model predictions were compared to observations using a contingency table with the following categories:

• True Positives (TP): Correctly predicted wet cells (M1B1)

• True Negatives (TN): Correctly predicted dry cells (M0B0)

False Positives (FP): Predicted wet but dry benchmark cells (M1B0)
 False Negatives (FN): Predicted dry but wet benchmark cells (M0B1)





From this classification, the following skill metrics were derived:

Hit rate index (H) = 
$$\frac{TP}{TP + FN}$$
 Equation 3

False ratio index (F) = 
$$\frac{FP}{TP + FP}$$
 Equation 4

Critical success index (C) = 
$$\frac{TP}{TP + FP + FN}$$
 Equation 5

Error bias index (E) = 
$$\frac{FP}{FN}$$
 Equation 6

395 These binary skill metrics complement the continuous accuracy measures and provide a comprehensive evaluation of the model's performance, particularly for assessing its capability to predict flooding extents.

#### 4 Results

## 4.1 Validation

## 4.1.1 Coastal water levels

Modeled still water levels from WY1942 until WY2022 were validated against gauge data. An example time series of 1 month of water level at the tide gauge station Seattle, WA (NOAA station #9447130), including the decomposition in tide and NTR, is shown in Figure 3. Table 1 contains a summary of skill scores for still water level and tide of 2 NOAA gauges for 84 years of modeled water years in terms of RMSE, SCI, MAE, and bias. We estimate an RMSE of 14.0 to 17.1 cm and an SCI of 7.9 to 10.3%. Errors are driven by a combination of modeled tide and NTR. Tides are reproduced with an RMSE of 8.4 to 8.5 cm, indicating a contribution of approximately half of the error. While tides are generally more deterministic and "easier" to model, the tide signal is also much larger than NTR, so it is unsurprising that it contributes a large fraction of the error. Sources of overall water level discrepancy are driven by offsets in NTR (remote SLA and locally generated wind-driven surge; notice panel C in Figure 3), inaccuracies in bathymetry and/or frictional effects, or local baroclinic effects that are unaccounted for in a depth-averaged model without density differences driven by temperature and salinity.



410



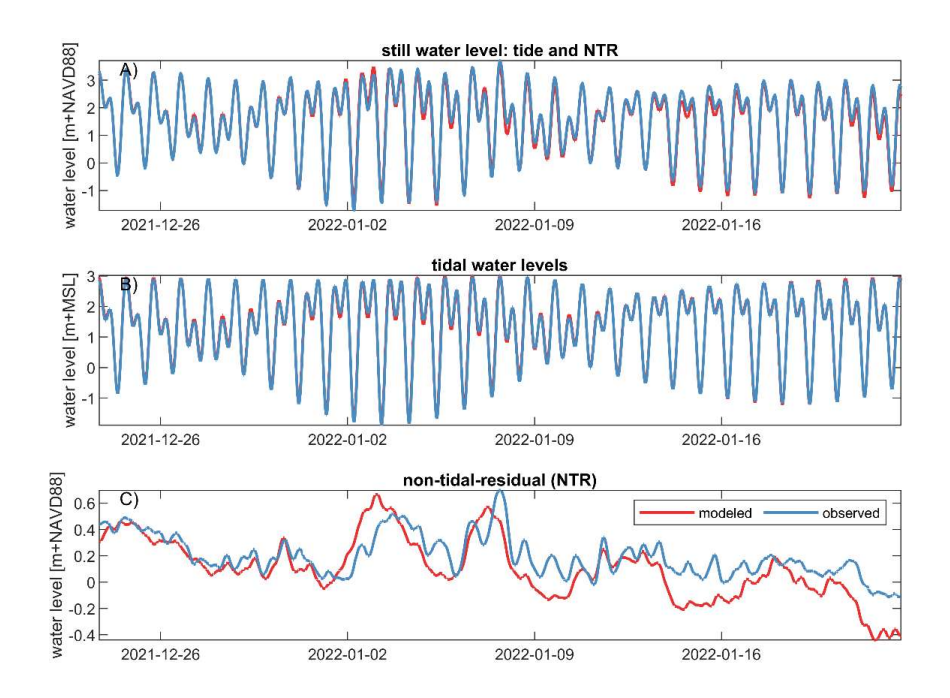


Figure 3. Comparison of coastal water levels at Seattle, WA (NOAA station #9447130): Comparison of modeled and observed still water levels for 1 month, including the decomposition into tidal (tide) and non-tidal residual (NTR) components. Panel (A) shows the observed and modeled still water levels, panel (B) highlights the modeled and observed tidal contribution, and panel (C) presents the NTR. Determination of the tidal signal was done in the same manner for both the modeled and observed signals.

415 Table 1. Comparison of skill scores for modeled water levels at Tacoma (NOAA station #9446484) and Seattle (NOAA station #9447130; also shown in Figure 3 and indicated here with a \*): Summary of skill metrics for still water levels and tide-only components at Tacoma and Seattle tide gauge stations. Metrics include Root Mean Square Error (RMSE), Scatter Index (SCI), Mean Absolute Error (MAE), and bias.

	9446484	9447130*
Name	Tacoma	Seattle
RMSE [cm]	14.0	17.1
SCI [%]	7.9	10.3
MAE [cm]	10.9	14.3
Bias [cm]	+2.3	+9.3
RMSE tide only [cm]	8.5	8.4
MAE tide only [cm]	6.8	6.7
Years of data	27	84

15





### 420 4.1.2 Inland water levels

Model water levels for October 2007 to the end of WY2022 were validated against gauge data. Two sample time series, each three months long, plot water levels at a streamgage on the Duwamish River (USGS station 12113390; U.S. Geological Survey, 2025) and on the Puyallup River (USGS station 12101500, Figure 4). Table 2 presents skill scores for five inland water levels across USGS streamgages for which records extended as far back as 15 years. Errors in the model result from a combination of tidal and riverine inflow. The influence of tides appears to be overestimated at both the Duwamish (Figure 4 - panel A) and the Puyallup (Figure 4 - panel B) stations. This overestimation is most likely a result of errors in riverine bathymetry, which allow tidal propagation too far upstream. This is apparent from modeling results, where at the Duwamish River USGS station (12113390) tidal oscillations are observed, but their modeled amplitudes are too large. Conversely, at the Puyallup River (USGS station 12101500), tidal effects are not observed, but the model simulates some tidal oscillation. Despite these disparities, the model captures the timing of heightened riverine discharges and associated stage increases. For the Duwamish River (USGS station 12113390), the peak flows are a day early in the model versus observations, while timing at the Puyallup River (USGS station 12101500) is well captured. Errors derived using the uMAE for the gauges range from 37 to 87 cm and represent the combined influence of tidal and riverine error components.

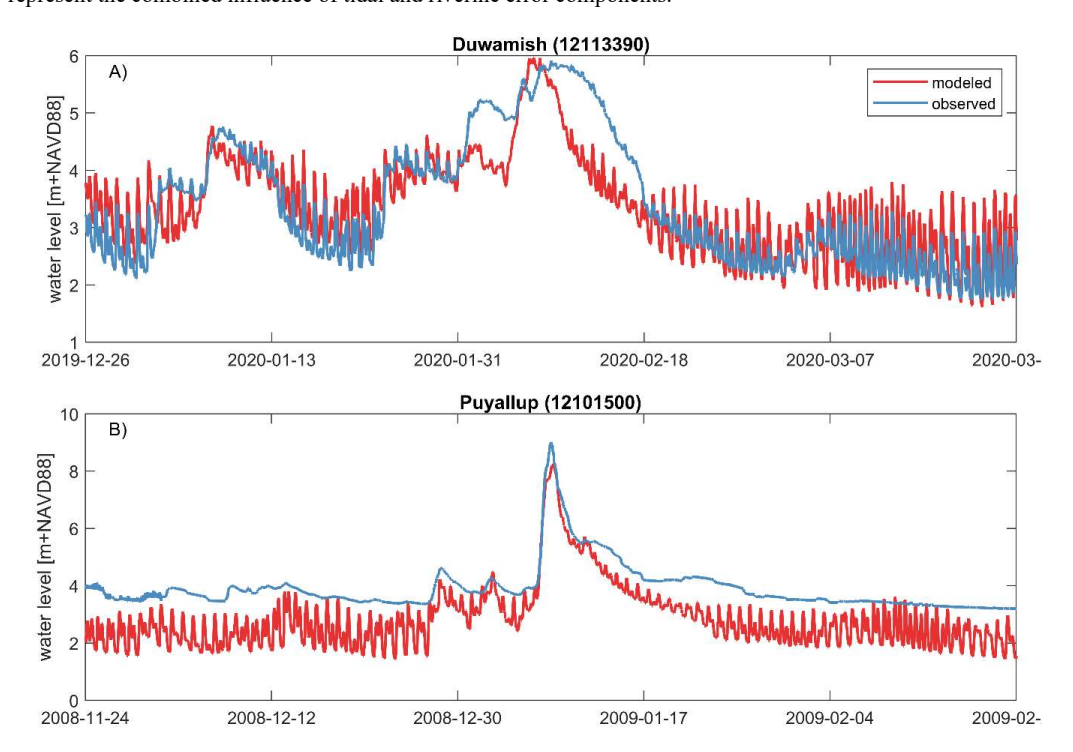






Figure 4. Modeled and observed inland water levels: Panel (A) shows water levels at a streamgage on the Duwamish River (USGS station 12113390), while Panel (B) presents water levels at a streamgage on the Puyallup River (USGS station 12101500; U.S. Geological Survey, 2025).

Table 2. Comparison of skill scores for modeled inland water levels at five USGS stations (U.S. Geological Survey, 2025):
Performance metrics for modeled water levels are provided for five gauges across the Puyallup and Duwamish watersheds. The number of years of available data for validation is also listed. Stations marked with an asterisk (\*) are reference locations discussed in Figure 4.

	12096500	12101500*	12113000	12113344	12113390*
Watershed	Puyallup	Puyallup	Duwamish	Duwamish	Duwamish
uRMSE [cm]	115.7	69.6	48.7	86.6	58.9
uMAE [cm]	87.2	53.2	37.6	53.2	38.8
Years of data	15	15	15	11	9

#### 4.1.3 Flood extents

The 2-meter resolution flood model was used to determine the 100-year flood extent (1% AEP) in King and Pierce Counties.

The model was compared to FEMA's SFHA, examining 38.25 million grid cells for King County and 45.69 million for Pierce County. The Hit Rate Index (H) was 0.746 for King County and 0.827 for Pierce County, indicating that roughly 80% of FEMA-mapped flood areas were also identified by the model (Table 3). The Critical Success Index (C), with weight for correct predictions but also weighing misses and false alarms, was narrowly lower (0.721 and 0.809, respectively), indicating minimal false alarms. In particular, the False Alarm Ratio (F) is minimal for each of the counties (0.044 for King and 0.026 for Pierce).

The small Error Bias Index reveals that the model underestimates the extent of flooding relative to FEMA maps. Overall, some discrepancies between these two products are expected because the methodologies differ substantially.

Figure 5 demonstrates this performance spatially and highlights the mixed agreement between SFINCS-modeled and FEMA-reported flood extents. Panel A highlights the South Park neighborhood in Seattle, WA, where model results show extensive flooding along the Duwamish Waterway while FEMA maps suggest no flooding despite its history of inundation (refer to Section 2 'Study Site'). Panel B shows the Oro Bay coastal region on Anderson Island, WA, where the model and FEMA alignment are mixed, with both areas flooded by SFINCS and not by FEMA, and vice versa. Panel C presents an upstream portion of the Green and Duwamish Rivers near Kent, WA, where both the model and FEMA show strong agreement across a broad river floodplain.

460

Table 3. Summary of flood extent validation metrics comparing modeled 100-year flood extents with FEMA Special Flood Hazard Areas (SFHA) for King and Pierce Counties. Metrics include the Hit Rate Index (H), False Alarm Ratio (F), Critical Success Index (C), and Error Bias Index (E), based on pixel-level agreement.

King County	Pierce County





Hit rate index (H)	0.746	0.827
False Alarm Ratio index (F)	0.044	0.026
Critical Success Index (C)	0.721	0.809
Error Bias Index (E)	0.134	0.127
Number of total cells analyzed [M]	38.25	45.69

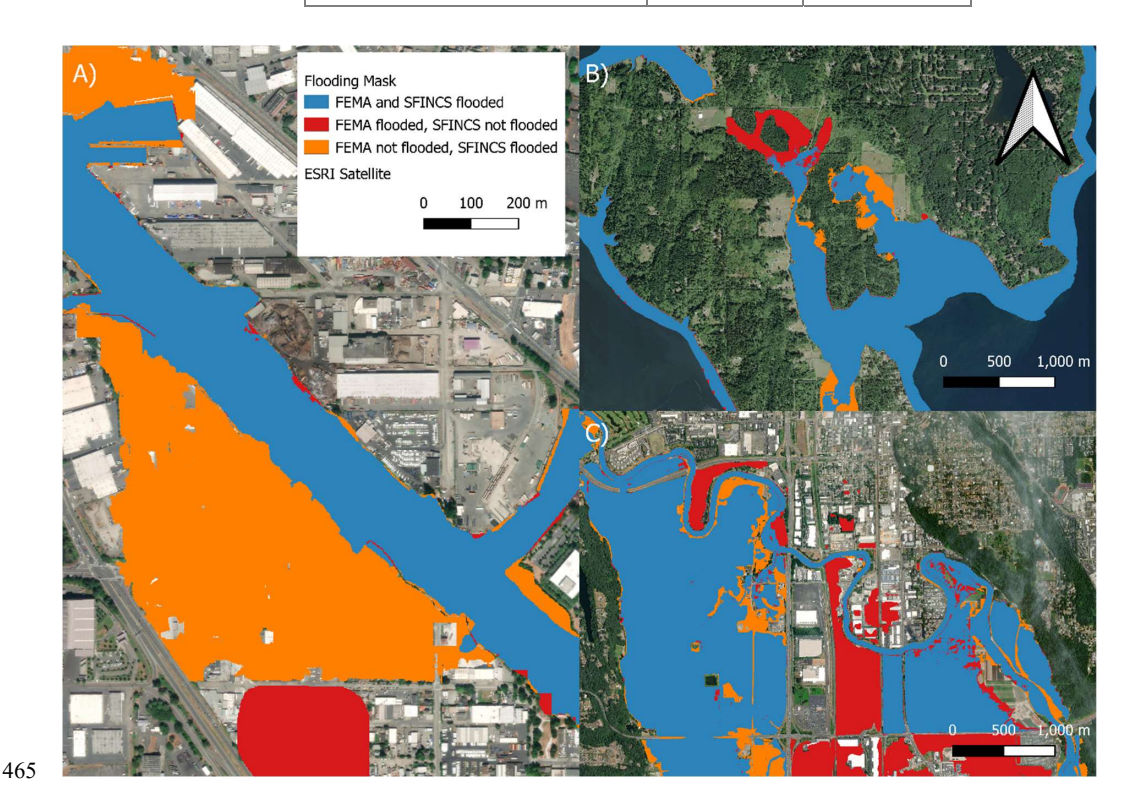


Figure 5. Comparison of 100-year modeled flood extent by SFINCS with FEMA Special Flood Hazard Areas (SFHA) in selected locations across King and Pierce Counties, Washington. Colors represent flood agreement classification: blue for hits (both SFINCS and FEMA indicate flooding), red for misses (flooding observed by FEMA but not captured by SFINCS), and orange for false alarms (SFINCS predicts flooding not identified in FEMA maps). Panel A: South Park neighborhood in Seattle, WA, adjacent to the Duwamish Waterway. Panel B: Oro Bay on Anderson Island, WA, illustrates a coastal setting. Panel C: A reach of the Green/Duwamish River near Kent, WA. Background: ESRI Satellite Imagery. Sources: Esri, Maxar, GeoEye, i-cubed, USDA FSA, USGS, AEX, Getmapping, Aerogrid, IGN, IGP, swisstopo, and the GIS User Community.

## 4.1.4 Moment of flooding

Unlike traditional flood hazard assessments that rely on predefined design events (e.g., the "100-year flood"), our approach
uses the CFRM (Continuous Flood Response Modeling) framework. Both coastal and riverine processes over decades of
climate forcing resolve extremes on a grid-cell basis rather than from a single event. This approach could complicate

Public domain. CC0 1.0.



480



communication with stakeholders who are used to the FEMA event-based framework, but can provide robust information about flooding. Retrieval of the exact date and time when peak flooding occurred across space supports validation and analysis of the spatially varying forcing causing the extremes. This approach also provides a spatially robust characterization of extremes. The forcing (and type of event) that causes extremes varies spatially across regions. The most natural example of this is the transition from coastally driven to compound to fluvially driven forcing while moving up a river. A single "design storm" modelling approach does not capture this spatial transition in what events are causing extremes.

To support an in-depth analysis of the moment of flooding, a new output variable was introduced into the SFINCS model that records the timestamp of the maximum water level for each grid cell. This new variable enables a spatially explicit assessment of the dominant flood-generating event across the landscape. The resulting analysis is shown in Figure 6, which maps the peak water levels to specific historical flood events and is summarized in Table 4.

An event on December 28, 2022, caused the most widespread flooding in the area. The occurrence was driven by the combined effects of high coastal water levels and high discharge and is colloquially referred to as a 'King Tide' event. This King Tide event produced the highest water level for the hindcast period in 78.5% of King County grid cells and 83.9% of Pierce County grid cells (blue areas of Figure 6). One of the most substantial impacts successfully duplicated by the model was on the Duwamish River in Seattle's South Park neighborhood, where business and urban areas were flooded. NOAA tide gauge #9447130 in Seattle recorded water at 3.88 m NAVD88 at 17:00 on 27 December, while SFINCS simulated a high of 4.03 m 495 NAVD88 at 16:20, indicating a close match in amplitude and time. The model also captured other critical events. For example, the event on January 8-9, 2009, led to significant riverine flooding along the Green River, reached a maximum water level in 7.2% of King County grid cells, and was preceded by warnings of flooding that said the City of Carnation might become an island (KOMO, 2020). There was a local urban flooding incident on December 4, 2007, along the lower Duwamish River, which contributed to 2% of peak modeled extents in King County. Maximum flooding in 7% of cells, particularly in the Nisqually River region, occurred during the flood of November 25–26, 1990, in Pierce County. The event, which took place over Thanksgiving week, resulted in two fatalities and involved large-scale evacuations (USGS, 1994). The second largest event in the record, based on the number of cells reaching their maximum extent on this date, occurred in December 5, 1975, as a severe winter storm with heavy rain and snowmelt, resulting in widespread riverine flooding within the Green, Nisqually, and Puyallup River systems (STARR, 2015). This 1975 event contributed 10.2% to the highest modeled water levels in King 505 County and 6.7% in Pierce County. These events, although less dominant than the 2022 'King Tide' event, demonstrate the diverse mechanisms and regional variation of historical flood drivers in the Pacific Northwest.





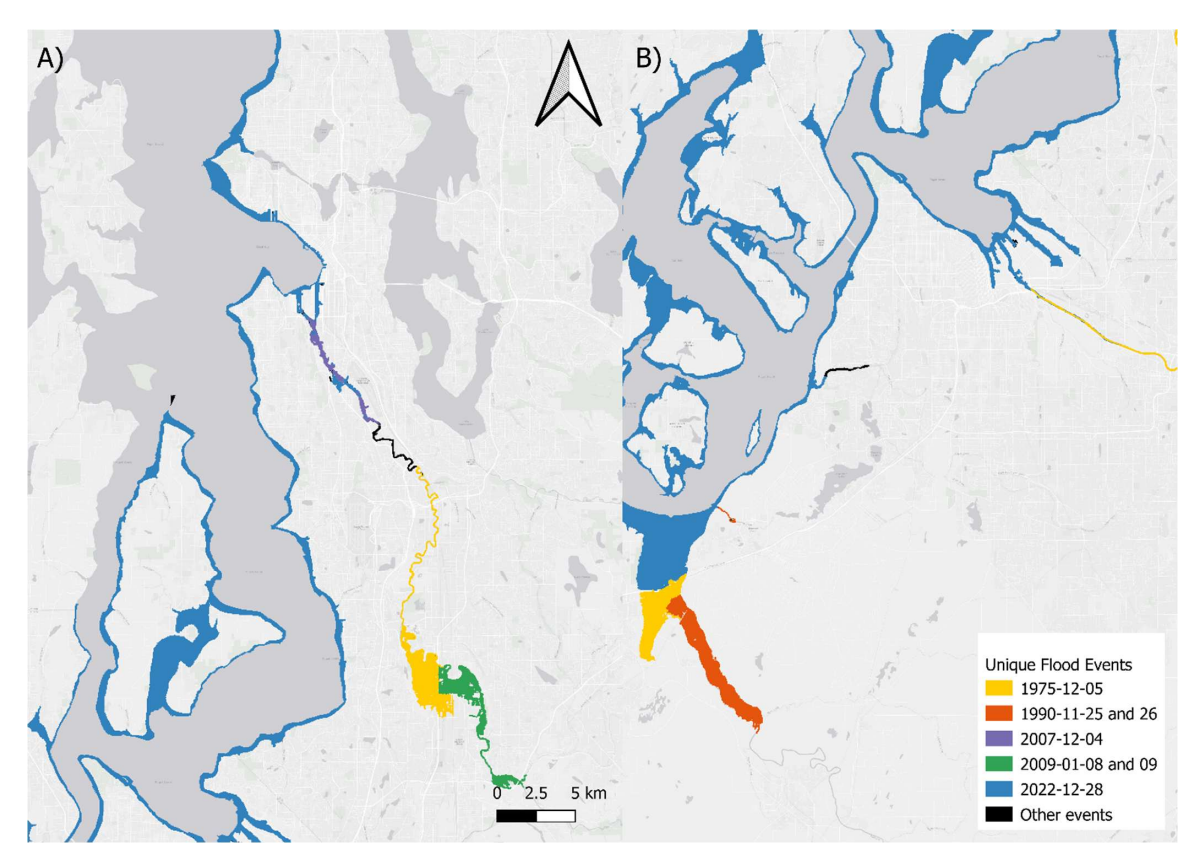


Figure 6. Spatial pattern of individual flood extents associated with specific historical events in King (panel A) and Pierce Counties (panel B). The colors represent the dominant flood event at each location, determined by the peak modeled flood depth timing. The map illustrates the temporal and spatial heterogeneity of flood-generating mechanisms in the region. Background: Esri Gray Canvas basemap. Sources: Esri, HERE, Garmin, FAO, NOAA, USGS, EPA, NPS, and the GIS User Community.

Table 4. Summary of the most influential flood-generating events and their areal contribution to peak flood limits in King and Pierce Counties. Percentages refer to the proportion of the total area flooded to which the respective event attained the highest modeled water level. The December 28, 2022, coastal flood event caused the majority of flood extents in both counties, and other events—such as the 1975 Green and Nisqually Rivers flood, and the 2009 upper Green River flood—were more restricted in effect. The rest of the extent was influenced by other, less common events (not shown).

Date time	Areas effects	King County	Pierce County
2022-12-28	The majority of coastal areas across the areas of interest	78.5%	83.9%
2009-01-08 and 09	Green River / Duwamish River	7.2%	0.0%
2007-12-04	Downtown Seattle	2.4%	0.0%
1990-11-25 and 26	Upstream Nisqually	0.0%	7.2%





1975-12-05	Portions of GreenNisqually, and Puyallup Rivers	10.2%	6.7%
	All other events	1.7%	2.2%

#### 4.2 Flood hazards

### 4.2.1 Current climate conditions

Flood extents increase consistently with return period in both King County (Figure 7, panel A) and Pierce County (panel B), illustrating the growing impact of rarer and more intense flood events. In King County, flood extents grow gradually for lower return periods (1 to 10 years), particularly in the severe (red, >1 m depth) and hazardous (orange, >30 cm) categories. For example, severe flooding increases from 9 hectares at the 1-year event to 656 hectares at 10 years. However, the growth becomes more substantial for higher return periods, especially for nuisance flooding (blue, >10 cm), which reaches 1,150 hectares at the 100-year event. In Pierce County, total flooded areas are generally larger across all severity levels. Nuisance flooding, for instance, increases from 24 hectares (1 year) to 1,493 hectares (100 years), while severe flooding grows from 13 hectares to 931 hectares over the same range. The rate of increase slows after moderate events (10–20-year return periods), but flood extent continues to grow with larger return periods, indicating that flood-prone areas are not yet fully saturated.

The final bar in each panel represents the Expected Annual Flooded Area (EAFA), a probability-weighted average integrated across return periods from 1 to 100 years. EAFA provides a more holistic and policy-relevant measure of flood hazard, accounting for both event frequency and severity, and is comparable to translating damages to flood risk with the Expected Annual Damages (EAD, Rosbjerg, 2024). In King County, EAFA is estimated at 56 hectares for severe flooding, 160 hectares for hazardous flooding, and 200 hectares for nuisance flooding. In Pierce County, EAFA values are higher with 250, 531, and 644 hectares for severe, hazardous, and nuisance flooding, respectively.

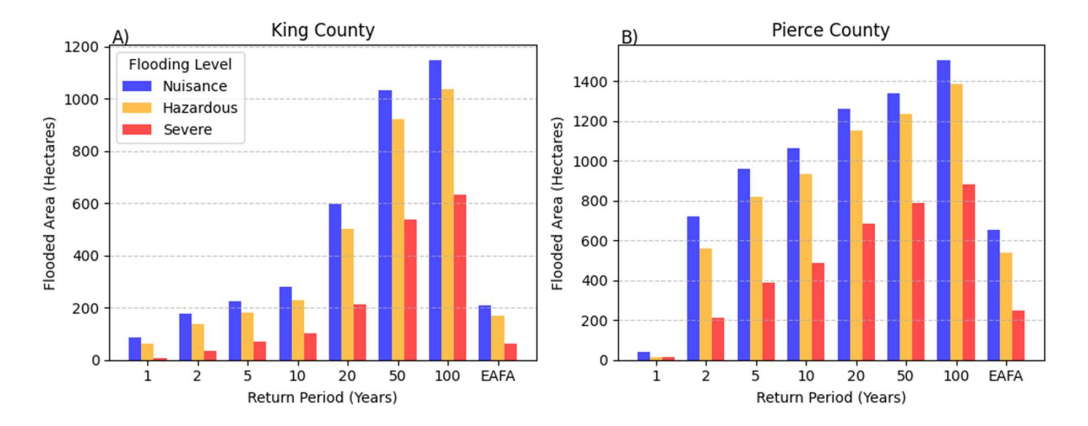






Figure 7. Flooded area (in hectares) as a function of return period for three flood severity levels in King County (panel A) and Pierce County (panel B) under current climate conditions. Flood severity is classified as severe (red), hazardous (orange), and nuisance (blue). Return periods range from 1 to 100 years, with the final bar labeled EAFA representing the Expected Annual Flooded Area, a probability-weighted integration of flood extents across all return periods. Grid cells that are flooded during daily tidal conditions are removed.

The results provided in this subsection so far were computed using the CFRM approach. However, deterministic design events are often used in practice. An example is the simulation of the 10-year flood based on historical storm records. At Seattle (station #9447130), the December 5, 1967, event produced a height of 3.62 m NAVD88 and can be considered the 10-yr event based on the Weibull plotting position (Weibull, 1939). When we ran this event through our model and compared the results with the CFRM-based estimate for 10 years, we determined that coastal-zone differences were moderate (simulated high water level at Seattle of 3.72 m NAVD88), giving similar local flood areas. However, further inland along the coastal-riverine boundary, differences grew significantly. Peak water levels were up to 0.5 m higher in the Duwamish River, flooding a much larger area under the deterministic single-event design approach than under the CFRM method. The mean absolute difference between the two methods was 19 cm and 15 cm, respectively, in King and Pierce Counties. These results demonstrate the importance of the selection of the statistical approach in determining extreme-water-level estimates and, by extension, the spatial extent of flood inundation.

#### 4.2.2 Future climate conditions: sea level rise versus climate change

To evaluate how SLR and future climate conditions influence hazardous flooding (≥30 cm water depth), we analyzed four scenarios: (1) current climate with no SLR, (2) current climate with 1.0 m SLR, (3) future climate with no SLR, and (4) future climate with 1.0 m SLR (Figure 8). This approach allows isolation of SLR effects vs. climate-change effects. Results are analyzed using the same return periods and the EAFA as in Section 4.2.1.

The results indicate that SLR is the dominant driver of increased hazardous flooding. In King County, EAFA increases from 161 hectares for the current situation to 787 hectares due to 1.0 m of SLR. Similarly, Pierce County shows an increase from 529 to 931 hectares. These increases are similar for the 10-year event, which nearly increases fivefold in King County (from 234 ha to 1,241 ha) and increases by more than 50% in Pierce County (from 913 ha to 1,353 ha). The absolute influence of SLR is particularly pronounced at higher return periods, while the relative increase is largest at lower return periods.

In contrast, future climate forcing alone results in negligible to slightly negative changes in hazardous areas. In both counties, EAFA values stay approximately the same (161 to 160 ha for King County and 529 to 531 ha for Pierce County for current versus future climate, respectively). Moreover, in King County, the 20-year return period hazardous area *decreases* from 531 ha to 481 ha (-9%), while in Pierce County, it *increases* from 1,065 ha to 1,071 ha (+1%). These results suggest that the future climate conditions modeled (up to 2050) do not intensify but rather slightly reduce flooding. This is an important reminder that climate change (unlike SLR) does not always mean higher flood risk.



585

When combining both SLR and future climate (Scenario 4, magenta color in Figure 8), results show only marginal differences from SLR alone (Scenario 2, green color in Figure 8), reinforcing that SLR is the overwhelming driver of increased hazardous flooding. In King County (Figure 8A), the EAFA in Scenario 4 is 787 hectares, ~7% below the EAFA for Scenario 2, which resulted in 738 hectares. In Pierce County (Figure 8B), EAFA increases by ~2% (931 ha vs. 954 ha for Scenarios 2 and 4, respectively). Across all modeled return periods, King County shows decreases at lower return periods (-21% to -1% for 1–10 years) but increases at higher return periods (+22% at 20 years and +15% at 50 years), while Pierce County consistently shows small increases of up to ~9%.

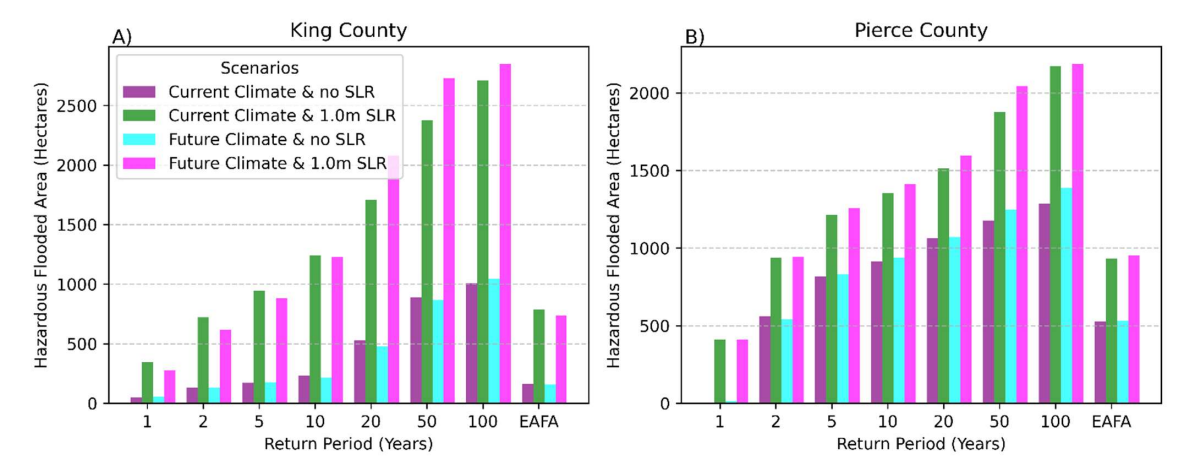


Figure 8. Flooded area (in hectares) as a function of return period in King County (panel A) and Pierce County (panel B) under 4 different climate and sea level scenarios. Return periods range from 1 to 100 years, with the final bar labeled EAFA representing the Expected Annual Flooded Area - a probability-weighted integration of flood extents across all return periods.

We computed EAFA focused on the hazardous severity class (>30 cm flooding) for King and Pierce Counties as a function of 7 SLR scenarios and accounting for model uncertainty (Table 5). Analysis reveals a threshold in EAFA hazards between roughly 100 cm and 150 cm of SLR, with median hazards increasing by roughly 13-fold in King County and 3-fold in Pierce County relative to the present-day. This suggests that SLRs exceeding ~1 m, large new areas of low-lying land (e.g., currently just above the present flood zone) become vulnerable, especially in King County. Hazard increase is gradual below this threshold, but above this threshold, absolute values for EAFA increase steeply. For example, by 300 cm, EAFA ranges from 4,520 to 6,408 hectares in King County and 3,205 to 4,509 hectares in Pierce County. Uncertainty ranges are largest, in absolute terms, at 200 cm SLR for both King and Pierce Counties, while proportionally they peak at 100 cm in King County and 50 cm in Pierce County. These findings demonstrate the model's sensitivity to thresholds. However, at SLR larger than 200 cm, when in absolute terms, uncertainty is large, the proportional spread diminishes, indicating consensus among model scenarios.





Table 5. Hazardous flooding class (> 30 cm water depth) Expected Annual Flooded Area (EAFA) for King and Pierce Counties under seven sealevel rise (SLR) scenarios. SLR is expressed relative to the mean sea-level in 2005 (cm). All EAFA values are in hectares (ha). "Low" and "High" represent the lower- and upper-bound estimates from the Low hazard and High hazard uncertainty simulations (refer to Section 3.2.2), respectively, while "Median" refers to the central estimate.

	King [ha]			Pierce [ha]		
SLR [cm]	Low	Median	High	Low	Median	High
0	61	160	411	343	531	773
25	91	226	639	372	608	935
50	126	319	1,046	412	685	1,240
100	243	738	2,294	577	954	2,101
150	490	2,168	3,814	776	1,661	2,941
200	1,247	3,696	4,757	1,100	2,698	3,504
300	4,520	5,422	6,408	3,205	3,830	4,509

### 5 Discussion

615

To facilitate reading and ease of understanding, the discussion is divided into five subsections: (1) model performance and validation, (2) benefits of Continuous Flood Response Modeling (CFRM) in determining extremes versus traditional design-event methods; (3) computational trade-offs and limitations; (4) the utility of the Expected Annual Flooded Area (EAFA) metric in planning and risk-informed decision-making; and (5) future directions and adaptation research implications. This organization allows both the methodological improvements and practical applicability of the proposed modeling framework to be considered clearly.

# 5.1 Model performance and validation

The validation results demonstrate that the presented workflow skillfully reproduces coastal water levels (Section 4.1.1), inland water levels (Section 4.1.2), flood extents (Section 4.1.3), and timing of flooding (Section 4.1.4). Strong model performance is attributable to (1) the nesting of the overland flow domains within large-scale coastal and inland models that provide reliable boundary conditions and (2) the inclusion of relevant bathymetric features. Computational efficiency was a key design consideration to enable the usage of the CFRM framework and simulation of thousands of years (i.e., 7+2 SLR scenarios, 3 uncertainty layers, 2 domains, 100 years = 5400 simulations) of hydrodynamic processes. However, this consideration came with trade-offs: the model resolution was constrained to  $50\times50$  meters, with fine-scale flood features resolved using subgrid lookup tables based on a 1-meter DEM. We acknowledge that this tradeoff sacrifices, to some degree, the accuracy with which water levels are simulated (as gauged in the validation) for better fidelity in extremes and compound events. For example, one

https://doi.org/10.5194/egusphere-2025-4909

Preprint. Discussion started: 11 November 2025

Public domain. CC0 1.0.





week of simulation at very high resolution and with a full physics model would produce better validation statistics, but at the cost of requiring an event-based strategy that sacrifices fidelity in description of the extremes. This loss of accuracy (decreased power to statistically capture extremes) is harder to quantify but must be considered in the choice of a specific workflow.

# 5.2 Benefits of Continuous Flood Response Modeling (CFRM) for extreme events

From an extreme value analysis (EVA) perspective, the chosen approach provides important advantages. The first is that a continuous 100-year simulation approach enables a cell-by-cell empirical EVA without requiring the fitting of statistical distributions. Fitting of an EVA statistical model adds significant uncertainty to predicted extremes, and an EVA model (statistical in nature) will underperform relative to a physics-informed model at constraining extremes. Second, abandoning the traditional application of a single, one-off "100-year" design event is particularly warranted in dynamic coast-riverine settings where diverse combinations of drivers can produce equally hazardous, yet spatially distinct, flood effects. As shown 625 in Figure 6, a succession of diverse storms contributed importantly to the historical flood record, so a single, representative "100-year event" might mistakenly identify vulnerable areas. Our comparison in Section 4.2.1 also makes the point that deterministic 10-year design events produced local flood levels that were locally as much as 0.5 m higher than the CFRMderived 10-year estimate, demonstrating how extreme water levels and flood extents depend on the method used to derive 630 them. Finally, the continuous time-series approach naturally captures compound extreme events where coastal and river forcings are phase-lagged or decoupled, for example, a coastal surge with a peak days apart from a river flood would most likely be underestimated by one design storm. As a result, CFRM provides a robust and spatially representative basis for flood hazard assessment and planning.

Secondly, traditional design events typically represented by a single, static, deterministic "100-year" scenario, may not effectively model dynamic coastal–riverine systems where multiple drivers can produce diverse flood outcomes. As illustrated in Figure 6, several distinct storms contributed significantly to the historical flood record. Modeling the region with a single design event would therefore underpredict extremes at some locations where the incorrect 100-year storm is being modeled. In particular, the difference between the Continuous Flood Response Modeling (CFRM) and the deterministic 10-year design event revealed a MAE of ~19 cm with local differences as high as 0.5 m (Section 4.2.1). Additionally, a continuous time-series approach improves consideration of compound extreme events where fluvial and coastal side forcing may be phase-lagged or even decoupled.

# 5.3 Limitations and computational trade-offs

The chosen model configuration eproduces flooding well across most of the domain, achieving high spatial agreement with FEMA flood extents (hit rates: 0.75–0.83). However, in narrow rivers the model introduces localized edge effects that results in overestimation of the river footprint. These effects are driven by the relatively coarse modeling resolution in combination with the usage of weirs. However, these limitations are consistent with other subgrid modeling approaches (e.g., van Ormondt

https://doi.org/10.5194/egusphere-2025-4909

Preprint. Discussion started: 11 November 2025

Public domain. CC0 1.0.



670



et al., 2024). Incorporating subgrid bathymetry is rapidly becoming the new standard because it allows the user to account for more information per grid cell and therefore improves the accuracy of the simulation. Subgrid bathymetry refers to storing and using high-resolution elevation information (e.g., 1 m DEM data) inside each larger model grid cell (e.g., 50 m) and allows the user to simulate on coarser resolutions without significant loss of accuracy. Coastal boundary mismatches are within the range of previous efforts (e.g., Nederhoff et al., 2024), driven by both differences in tides and the NTR. The persistent bias at Seattle (#9447130) is notable and is hypothesized to result from steric density-driven effects that are not accurately captured by the regional model (Parker et al., in preparation). Inland water level offsets stem from uncertainties in total inflow estimates (Buitink et al., 2025) and inaccurate riverine bathymetry. In some cases, bathymetry was manually deepened to improve hydraulic connectivity (refer to Section 3.2). Good-quality bathymetric data at the riverine–coastal interface remains a challenge over much of the globe, despite this interface being one of the most vulnerable regions to SLR and climate-driven change.

Simplifications in the model and assumptions were required by computational and scale constraints. The SFINCS model used in this study has no stationary wave solver, infragravity waves, rainfall-runoff processes, sediment transport, or morphological change. Also, the SFINCS domains were not calibrated; default parameter values were used throughout. Future calibration of parameters such as bottom friction could improve model accuracy. Wave setup was prescribed at the offshore boundary using a simple estimate of 20% of the wave height, similar to Vousdoukas et al. (2018), although the accuracy was not assessed.
 Observations of wave setup in mixed sediment, low wave energy environments are sparse, and a case study with more comprehensive data at the exposed shoreline could provide further insights. The absence of high-fidelity wave and runoff modeling likely leads to the underestimation of flood hazards in both coastal and inland zones. A comparison with FEMA 100-year flood maps yielded hit rates between 0.75 and 0.83, though the bias index (0.13) indicates a tendency to underpredict flood extent.

While the CFRM approach was chosen for its multiple advantages, it is important to note that we simulated only 100 years of hydrodynamic forcing; therefore, by definition, the maximum flood extent observed corresponds to the 100-year event. This relatively low number of simulated years restricts the statistical confidence within the higher end of the extreme value frequency and does not identify more rare combinations. Extending the length of the simulation would increase the reliability of the higher return period estimates and allow for a more comprehensive sampling of tidal and storm interactions. The length of the simulation was not increased in the present study due to computational cost constraints, which remain a limit on long-duration, high-resolution flood simulation. However, this framework permits temporal analysis of flooding, which can be used for validation (Section 4.1.4) and planning.

Public domain. CC0 1.0.



690

705



# 5.4 Expected Annual Flooded Area (EAFA) and planning relevance

The Expected Annual Flooded Area (EAFA) is a more insightful, probability-weighted value of flooded area. EAFA captures contributions over the full range of return periods and is potentially a better tool for planners than fixed-frequency areas of flooding. There is a growing consensus that deterministic flood maps, while useful for regulation, are not sufficient for climate-informed planning (Wing et al., 2022). Binary discretised results (flooded or not flooded) for a single storm do not portray the gradient of risk over return periods or the probabilistic nature of flooding. EAFA avoids these restrictions by providing a scalable, continuous depiction of flood hazard that is better adapted for cost-benefit analysis and resilience planning.

Use of EAFA to estimate spatial flood extent is conceptually equivalent to the Expected Annual Damage (EAD) used in economic risk assessment by agencies such as FEMA (Rosbjerg, 2024) to estimate financial damages and is starting to be used more frequently (e.g., Vousdoukas et al., 2023). However, by merging EAFA with exposure layers, spatial patterns of expected annual impact can be estimated. This synthesis can enable agencies and municipalities to identify high-hazard areas, rank adaptation investments, and evaluate the performance of proposed interventions over time. EAFA is not meant to substitute but to supplement and enrich the planning and readiness of the community. Incorporation of EAFA in long-term planning reports, climate change adaptation plans, and capital investment plans can transform flood management from event-based, static models to response-based, dynamic risk management.

#### 695 5.5 Future research and adaptation implications

This paper considered future flood risk under climate change and SLR scenarios, but not morphological change or societal growth like population increase and new infrastructure. The natural system is expected to respond dynamically to these pressures; for instance, shoreline and bluff retreat are widely projected under rising seas (e.g., Vitousek et al. 2017). The built system will additionally adapt to changing hazards, so experienced flooding will be directly influenced by the adaptation measures taken as communities respond to the changing natural system.

Our findings indicate that SLR is a much more significant driver of future flood hazard in King and Pierce Counties than other climate change-related factors, such as changes in storm patterns, for the period assessed (through 2050 using the HighResMIP climate ensemble). Somewhat counterintuitively, the simulations show reduced flooding under future climate forcing alone without SLR. For this study, projected climate changes were derived using a cumulative distribution function (CDF) correction applied to the ensemble mean of 7 high-resolution CMIP6 models, following Parker et al. (in preparation). The relatively subdued or even negative storminess-driven changes in EAFA and return period flood extent under future climate forcing (in the absence of SLR) must be interpreted in the context of both methodological and climate-signal considerations. Similar patterns were observed when assessing projected changes in storm surge and wave climate around the Salish Sea using the same seven-member HighResMIP CMIP6 ensemble (Parker et al., in preparation). High spread among individual CMIP6

Public domain. CC0 1.0.





members was noted, with several models producing consistently smaller changes than the others; when averaged, these model results weakened the ensemble-mean signal. This high model variability suggests that the ensemble mean may underestimate potential changes captured by some members. A second important point is the time-horizon mismatch between the climate-change and SLR scenarios used here. The HighResMIP CMIP6 simulations run only until 2050, whereas SLR increments used in our sensitivity analysis could be representative of longer-term futures. As a consequence, the relative magnitude of storminess change and SLR is not directly comparable. These findings underscore the importance of caution in interpreting ensemble-mean climate change effects on extremes in the Salish Sea, at least when confined to mid-century time frames. Longer-term, high-resolution climate forcing data sets—considering both hydrologic and oceanographic inputs—would be required to directly compare century-scale SLR projections with storminess change on the same time scales.

720

725

735

Further modelling efforts could include physical processes not simulated here, such as wave runup and rainfall-runoff routing. Higher spatial resolution and more accurate representation of hydrologic and land-sea interaction processes could enhance model fidelity, particularly in compound flood settings. More detailed representation of urban drainage infrastructure and dynamic groundwater-surface water interactions would be needed for more complete inland flood simulations. Finally, combining EAFA or other hazard metrics with dynamic exposure layers (population, assets, critical infrastructure, etc.) would aid in the development of actionable, risk-based adaptation plans.

#### 6 Conclusion

This study addressed growing flood risk in Pacific Northwest estuarine systems, where sea-level rise and changing storm systems threaten coastal and riverine communities. Traditional flood estimations with design events (e.g., FEMA's 100-year flood) would likely not account for the compound and spatially varying nature of extreme water levels. In an attempt to overcome this limitation, we utilized a Continuous Flood Response Modeling (CFRM) approach to simulate overland flooding in Pierce and King Counties using high-resolution SFINCS models. The approach incorporated many decades worth of dynamic boundary forcing data (coastal water levels and riverine inflow), and spatially variable friction, bathymetry, land cover, and topography to simulate dynamic flood processes. This approach enabled empirical determination of extreme recurrence at per-cell resolution sensitive to the combined effect of coastal and fluvial forcing and independent of statistical assumptions. Furthermore, the inclusion of a new innovative variable in SFINCS allowed accurate tracing of the timing of peak water levels, offering insights into dominant flood-generating events both spatially and temporally, and offering additional opportunities for validation.

Validation showed model performance where coastal water levels were simulated with errors of 14 to 17 cm at two NOAA gauges and inland water levels with RMSEs of 49–116 cm at five USGS streamgages. Agreement with FEMA flood maps was high (hit rate indices of 0.75 in King County, 0.83 in Pierce County) with a slight underestimation bias (error bias index ≈0.13).

https://doi.org/10.5194/egusphere-2025-4909

Preprint. Discussion started: 11 November 2025

Public domain. CC0 1.0.





Under current climate conditions, the model predicted substantial spatial variation in flood hazards. The Expected Annual Flooded Area (EAFA), a probability-weighted sum of all return periods, ranged from 56 to 200 hectares in King County and 250 to 644 hectares in Pierce County based on flood severity. Modeled future climate conditions showed that SLR is the dominant variable causing increased flood extent, while simulated climate forcing changes without SLR had negligible or even slightly negative effects on area flooded. One important observation in these runs is the presence of a threshold in the relationship between SLR and flood risk. Particularly, we detected the largest increases in flood risk between 100 and 150 cm SLR. The analysis also revealed that accounting for all relevant drivers (tide, surge, discharge) is essential for accurately predicting flood risk. A simplified, deterministic mapping approach based on a 10-year design flood resulted in flood depth errors of up to 0.5 meters and significantly different spatial extents.

These findings demonstrate the utility of CFRM in flood risk estimation. Furthermore, EAFA provides a quantitative and informative index to planners and policymakers, offering a more complete evaluation of flood risk than traditional single–return-period flood maps. Future research could incorporate other drivers, such as direct rainfall and wave behavior, and integrate flood hazard projections with exposure and vulnerability data to fully express risk.

#### 7 Declarations

**Conflict of interest**: The authors have no competing interests to declare that are relevant to the content of this article. Any use of trade, firm, or product names is for descriptive purposes only and does not imply endorsement by the U.S. Government.

Data Transparency: All data supporting the findings are available without restriction in Parker et al. (2025a and 2025b).

**Authorship**: KN developed the modeling framework and wrote the manuscript with major contributions from all co-authors. KP was the research lead and project coordinator, responsible for ensuring that key ideas and the scientific direction were accurately represented. EG contributed to the conceptualization of the project and was responsible for funding acquisition. All co-authors wrote the manuscript, reviewed, and approved the final manuscript.

Funding: The research was funded by the United States Environmental Protection Agency (EPA).

**Acknowledgments**: We appreciate USGS staff efforts in performing a thorough quality assurance/quality control evaluation of the model results. We also thank Jennifer Thomas and Tim Leijnse for their critical review, which improved the manuscript.

## 8 References

Abeysirigunawardena, D. S., Smith, D. J., & Taylor, B. (2011). Extreme sea surge responses to climate variability in coastal British Columbia, Canada. *Annals of the Association of American Geographers*, 101(5), 992–1010. https://doi.org/10.1080/00045608.2011.585929



805



- Ali, J., Wahl, T., Morim, J., Enriquez, A., Gall, M., & Emrich, C. T. (2025). Multivariate compound events drive historical floods and associated losses along the U.S. East and Gulf coasts. *Npj Natural Hazards*, *2*(1), 19. https://doi.org/10.1038/s44304-025-00076-5
  - Barnard, P. L., Erikson, L. H., Foxgrover, A. C., Hart, J. A. F., Limber, P., O'Neill, A. C., van Ormondt, M., Vitousek, S., Wood, N., Hayden, M. K., & Jones, J. M. (2019). Dynamic flood modeling essential to assess the coastal impacts of climate change. *Scientific Reports*, *9*(1), 4309. https://doi.org/10.1038/s41598-019-40742-z
- Barnard, P. L., van Ormondt, M., Erikson, L. H., Eshleman, J., Hapke, C., Ruggiero, P., Adams, P. N., & Foxgrover, A. C. (2014). Development of the Coastal Storm Modeling System (CoSMoS) for predicting the impact of storms on high-energy, active-margin coasts. *Natural Hazards*, 74(2), 1095–1125. https://doi.org/10.1007/s11069-014-1236-y
- Brogli, R., Heim, C., Mensch, J., Sørland, S. L., & Schär, C. (2023). The pseudo-global-warming (PGW) approach: methodology, software package PGW4ERA5 v1.1, validation, and sensitivity analyses. *Geoscientific Model Development*, 16(3), 907–926. <a href="https://doi.org/10.5194/gmd-16-907-2023">https://doi.org/10.5194/gmd-16-907-2023</a>
- Buitink, J., Dalmijn, B., Parker, K. A., Nederhoff, K., & Grossman, E. (2025). Wetter Winters, Drier Summers: Quantifying the change in hydrological response around the Puget Sound area using the wflow\\_sbm hydrological model and CMIP6 projections. [Preprint, under review at Hydrology and Earth System Sciences]. EGUsphere. https://doi.org/10.5194/egusphere-2025-4908
  - Couasnon, A., Eilander, D., Muis, S., Veldkamp, T. I. E., Haigh, I. D., Wahl, T., Winsemius, H. C., & Ward, P. J. (2020). *Measuring compound flood potential from river discharge and storm surge extremes at the global scale*. 489–504.
- Crosby, S. C., Nederhoff, K., VanArendonk, N., & Grossman, E. E. (2023). Efficient modeling of wave generation and propagation in a semi-enclosed estuary. *Ocean Modelling*, 102231. https://doi.org/10.1016/j.ocemod.2023.102231
- Dent, S., Wright, L., Mosley, C., & Housen, V. (2011). CONTINUOUS SIMULATION vs. DESIGN STORMS COMPARISON WITH WET WEATHER FLOW PREDICTION METHODS.

  \*\*Proceedings of the Water Environment Federation, 2000(4), 373–392. https://doi.org/10.2175/193864700785140836
  - Dethier, M. N., Raymond, W. W., McBride, A. N., Toft, J. D., Cordell, J. R., Ogston, A. S., Heerhartz, S. M., & Berry, H. D. (2016). Multiscale impacts of armoring on Salish Sea shorelines: Evidence for cumulative and threshold effects. *Estuarine, Coastal and Shelf Science*, 175, 106–117. https://doi.org/https://doi.org/10.1016/j.ecss.2016.03.033





- Falgout, J. T., Gordon, J., Lee, L., & Williams, B. (2025). *USGS Advanced Research Computing, USGS Hovenweep Supercomputer*. https://doi.org/10.5066/P927BI7R
- Federal Emergency Management Agency. (2025). National Flood Hazard Layer (NFHL): Special Flood Hazard Areas (SFHAs). Accessed August 19, 2025 on https://msc.fema.gov/nfhl

810

820

825

830

835

- Gori, A., Lin, N., & Xi, D. (2020). Tropical Cyclone Compound Flood Hazard Assessment: From Investigating Drivers to Quantifying Extreme Water Levels. *Earth's Future*, 8(12). https://doi.org/10.1029/2020EF001660
- Green, J., Haigh, I. D., Quinn, N., Neal, J., Wahl, T., Wood, M., de Ruiter, M., Ward, P., & Camus, P. (2025). A Comprehensive Review of 2 Compound Flooding Literature with a 3 Focus on Coastal and Estuarine Regions 4 5. 747–816. https://doi.org/10.5194/egusphere-2024-2247
  - Grossman, E. E., Tehranirad, B., Nederhoff, K., Crosby, S. C., Stevens, A. W., Van Arendonk, N. R., Nowacki, D. J., Erikson, L. H., & Barnard, P. L. (2023). Modeling Extreme Water Levels in the Salish Sea: The Importance of Including Remote Sea Level Anomalies for Application in Hydrodynamic Simulations. *Water (Switzerland)*, 15(23). https://doi.org/10.3390/w15234167
  - Haarsma, R. J., Roberts, M. J., Vidale, P. L., Senior, C. A., Bellucci, A., Bao, Q., Chang, P., Corti, S., Fučkar, N. S., Guemas, V., von Hardenberg, J., Hazeleger, W., Kodama, C., Koenigk, T., Leung, L. R., Lu, J., Luo, J.-J., Mao, J., Mizielinski, M. S., ... von Storch, J.-S. (2016). High Resolution Model Intercomparison Project (HighResMIP~v1.0) for CMIP6. *Geoscientific Model Development*, 9(11), 4185–4208. https://doi.org/10.5194/gmd-9-4185-2016
  - Hersbach, H., Bell, B., Berrisford, P., Hirahara, S., Horányi, A., Muñoz-Sabater, J., Nicolas, J., Peubey, C., Radu, R., Schepers, D., Simmons, A., Soci, C., Abdalla, S., Abellan, X., Balsamo, G., Bechtold, P., Biavati, G., Bidlot, J., Bonavita, M., ... Thépaut, J. N. (2020). The ERA5 global reanalysis. *Quarterly Journal of the Royal Meteorological Society*, *March*, 1–51. https://doi.org/10.1002/qj.3803
  - Homer, C., Dewitz, J., Jin, S., Xian, G., Costello, C., Danielson, P., Gass, L., Funk, M., Wickham, J., Stehman, S., Auch, R., & Riitters, K. (2020). Conterminous United States land cover change patterns 2001–2016 from the 2016 National Land Cover Database. *ISPRS Journal of Photogrammetry and Remote Sensing*, 162(February), 184–199. https://doi.org/10.1016/j.isprsjprs.2020.02.019
  - Hubbard, L. L. (1993). Floods of November 1990 in Western Washington (Issue Open-File Report 93-631). https://pubs.usgs.gov/of/1993/0631/report.pdf





- KOMO. (2020). City of Carnation could be "island" due to heavy rains, more flooding expected. https://www.seattlepi.com/local/komo/article/City-of-Carnation-could-be-island-due-to-heavy-15037967.php
  - Leijnse, T., van Ormondt, M., Nederhoff, K., & van Dongeren, A. (2021). Modeling compound flooding in coastal systems using a computationally efficient reduced-physics solver: Including fluvial, pluvial, tidal, wind- and wave-driven processes. *Coastal Engineering*, 163, 103796. https://doi.org/https://doi.org/10.1016/j.coastaleng.2020.103796
- Miller, I., Maverick, A., Johannessen, J., Fleming, C., & Regan, S. (2023). A Data-Driven Approach for Assessing Sea Level Rise Vulnerability Applied to Puget Sound, Washington State, USA. Sustainability (Switzerland), 15(6). https://doi.org/10.3390/su15065401
  - National Oceanic and Atmospheric Administration. (2025). NOAA Tides and Currents database. Accessed August 19, 2025.
- Nederhoff, K., Crosby, S. C., Van Arendonk, N. R., Grossman, E. E., Tehranirad, B., Leijnse, T., Klessens, W., & Barnard, P. L. (2024). Dynamic Modeling of Coastal Compound Flooding Hazards Due to Tides, Extratropical Storms, Waves, and Sea-Level Rise: A Case Study in the Salish Sea, Washington (USA). *Water*, 16(2), 346. https://doi.org/10.3390/w16020346
- Nederhoff, K., Leijnse, T. W. B., Parker, K., Thomas, J., O'Neill, A., van Ormondt, M., McCall, R., Erikson, L., Barnard, P. L., Foxgrover, A., Klessens, W., Nadal-Caraballo, N. C., & Massey, T. C. (2024). Tropical or extratropical cyclones: what drives the compound flood hazard, impact, and risk for the United States Southeast Atlantic coast? *Natural Hazards*. https://doi.org/10.1007/s11069-024-06552-x
- Nederhoff, K., Saleh, R., Tehranirad, B., Herdman, L., Erikson, L., Barnard, P. L., & van der Wegen,
  M. (2021). Drivers of extreme water levels in a large, urban, high-energy coastal estuary A case
  study of the San Francisco Bay. *Coastal Engineering*, 170, 103984.
  https://doi.org/10.1016/j.coastaleng.2021.103984
- O'Neill, A., Erikson, L. H., Barnard, P. L., Limber, P. W., Vitousek, S., Warrick, J. A., Foxgrover, A. C., Lovering, J., O'Neill, A. C., Erikson, L. H., Barnard, P. L., Limber, P. W., Vitousek, S., Warrick, J. A., Foxgrover, A. C., & Lovering, J. (2018). Projected 21st century coastal flooding in the Southern California Bight. Part 1: Development of the third generation CoSMoS model.

  Journal of Marine Science and Engineering, 6(2), 59. https://doi.org/10.3390/jmse6020059
- Oldford, G., Jarníková, T., Christensen, V., & Dunphy, M. (2025). *HOTSSea v1 : a NEMO-based physical Hindcast of the Salish Sea (1980 2018) supporting ecosystem model development*. 211–237. https://doi.org/https://doi.org/10.5194/gmd-18-211-2025





- Parker, K., Nederhoff, K., and Erikson, L.H., Hayden, M.K., Engelstad, A.C., Barnard, P.L., Grossman, E.E. 2025, CoSMoS (Coastal Storm Modeling System) modeled flood hazards for King County, Washington: U.S. Geological Survey data release, https://doi.org/10.5066/P13HYXKY
- Parker, K., Nederhoff, K., and Erikson, L.H., Hayden, M.K., Engelstad, A.C., Barnard, P.L., Grossman, E.E. 2025, CoSMoS (Coastal Storm Modeling System) modeled flood hazards for Pierce County, Washington: U.S. Geological Survey data release, https://doi.org/10.5066/P14U7EK2
  - Parker, K., Nederhoff, K., Engelstad, A., Grossman, E., & Erikson, L. (in preparation). Extreme coastal water levels in the Salish Sea simulated under CMIP6 high resolution scenarios. To be submitted to Natural Hazards and Earth System Sciences (NHESS).
- Rawls, W. J., Brakensiek, D. L., Saxton, K. E., Calhoun, F. G., Granger, M. A., & Breland, H. L. (1982). Estimation of Soil Water Properties. *Transactions of the ASAE*. https://doi.org/10.13031/2013.33720
  - Resio, D. T., & Irish, J. L. (2015). Tropical Cyclone Storm Surge Risk. *Current Climate Change Reports*, 1(2), 74–84. https://doi.org/10.1007/s40641-015-0011-9
- Roberts, M. J., Camp, J., Seddon, J., Vidale, P. L., Hodges, K., Vannière, B., Mecking, J., Haarsma, R., Bellucci, A., Scoccimarro, E., Caron, L. P., Chauvin, F., Terray, L., Valcke, S., Moine, M. P., Putrasahan, D., Roberts, C. D., Senan, R., Zarzycki, C., ... Wu, L. (2020). Projected Future Changes in Tropical Cyclones Using the CMIP6 HighResMIP Multimodel Ensemble. *Geophysical Research Letters*, 47(14), 1–12. https://doi.org/10.1029/2020GL088662
- Rosbjerg, D. (2024). Estimation of expected annual damage, EAD. *Proceedings of the International Association of Hydrological Sciences*, 385(4), 25–29. https://doi.org/10.5194/piahs-385-25-2024
  - Ruggiero, P. (2013). Is the Intensifying Wave Climate of the U.S. Pacific Northwest Increasing Flooding and Erosion Risk Faster Than Sea-Level Rise? *Journal of Waterway, Port, Coastal, and Ocean Engineering*, 139(2), 88–97. https://doi.org/10.1061/(asce)ww.1943-5460.0000172
- Santamaria-Aguilar, S., Maduwantha, P., Enriquez, A. R., & Wahl, T. (2025). *Large discrepancies between event- and response-based compound flood hazard estimates* (Issue May, pp. 1–25). https://doi.org/10.5194/egusphere-2025-1938
- Sebastian, A., Bader, D. J., Nederhoff, K., Leijnse, T., Bricker, J. D., & Aarninkhof, S. G. J. (2021). Hindcast of pluvial, fluvial and coastal flood damage in Houston, TX during Hurricane Harvey (2017) using SFINCS. *Natural Hazards*, 2017. https://doi.org/10.1007/s11069-021-04922-3





- Sisson, T. W., Vallance, J. W., & Pringle, P. T. (2001). Progress made in understanding Mount Rainier's hazards. *Eos, Transactions American Geophysical Union*, 82(9), 113–120. https://doi.org/https://doi.org/10.1029/01EO00057
- Soontiens, N., Allen, S. E., Latornell, D., Le Souëf, K., MacHuca, I., Paquin, J. P., Lu, Y., Thompson, K., & Korabel, V. (2016). Storm Surges in the Strait of Georgia Simulated with a Regional Model. *Atmosphere Ocean*, *54*(1), 1–21. https://doi.org/10.1080/07055900.2015.1108899
  - STARR. (2015). Washington Watershed Risk Assessment. https://starr-team.com/starr/RegionalWorkspaces/RegionX/Documents/Region X State Business Plans/Washington Watershed Risk Assessment.pdf
- 910 Sweet, W. V., Hamlington, B. D., Kopp, R. E., Weaver, C. P., Barnard, P. L., Bekaert, D., Brooks, W., Craghan, M., Dusek, G., Frederikse, T., Garner, G., Genz, A. S., Krasting, J. P., Larour, E., Marcy, D., Marra, J. J., Obeysekera, J., Osler, M., Pendleton, M., ... Zuzak, C. (2022). Global and Regional Sea Level Rise Scenarios for the United States. *NOAA Technical Report NOS 01*, 111 pp. https://oceanservice.noaa.gov/hazards/sealevelrise/noaa-nos-
- 915 Thomas, J. (2023). *Roles, Responsibilities, and Resources Related to Flooding in Seattles South Park Neighborhood*. South Seattle Emerald. https://southseattleemerald.org/news/2023/02/20/roles-responsibilities-and-resources-related-to-flooding-in-seattles-south-park-neighborhood
- Tohver, I. M., Hamlet, A. F., & Lee, S. Y. (2014). Impacts of 21st-Century Climate Change on Hydrologic Extremes in the Pacific Northwest Region of North America. *Journal of the American Water Resources Association*, 50(6), 1461–1476. https://doi.org/10.1111/jawr.12199
  - Tyler, D., Danielson, J. J., Grossman, E., & Hockenberry, R. (2020). Topobathymetric Model of Puget Sound, Washington, 1887 to 2017. *U.S. Geological Survey Data Release*. https://doi.org/10.5066/P95N6CIT
- U.S. Army Corps of Engineers. (1977). *Report on Floods of December 1975 and January 1976*. https://www.skagitriverhistory.com/Corps Docs/1977-06 USACE Report on Floods of 1975-12 AND 1976-01.pdf
  - U.S. Geological Survey. (1994). *Floods of November 1990 in Western Washington* (Issue Open-File Report 93-631). https://pubs.usgs.gov/of/1993/0631/report.pdf
- U.S. Geological Survey. (2025). USGS water data for the Nation: U.S. Geological Survey National Water Information System database. Accessed August 19, 2025, at https://doi.org/10.5066/F7P55KJN.





- van Ormondt, M., Leijnse, T., de Goede, R., Nederhoff, K., & van Dongeren, A. (2024). A subgrid method for the linear inertial equations of a compound flood model. In *Geoscientific Model Development* (Issue July, pp. 1–36). https://doi.org/10.5194/egusphere-2024-1839
- van Ormondt, M., Leijnse, T., Nederhoff, K., de Goede, R., van Dongeren, A., Bovenschen, T., & van Asselt, K. (2025). SFINCS: Super-Fast INundation of CoastS model. https://doi.org/https://doi.org/10.5281/zenodo.8038533
- van Verseveld, W. J., Weerts, A. H., Visser, M., Buitink, J., Imhoff, R. O., Boisgontier, H., Bouaziz, L., Eilander, D., Hegnauer, M., ten Velden, C., & Russell, B. (2024). Wflow\_sbm v0.7.3, a spatially distributed hydrological model: from global data to local applications. *Geoscientific Model Development*, 17(8), 3199–3234. https://doi.org/10.5194/gmd-17-3199-2024
  - Vitousek, S., Barnard, P. L., Limber, P., Erikson, L., & Cole, B. (2017). A model integrating longshore and cross-shore processes for predicting long-term shoreline response to climate change. *Journal of Geophysical Research: Earth Surface*, 122(4), 782–806. https://doi.org/10.1002/2016JF004065
- Viviroli, D., Sikorska-Senoner, A. E., Evin, G., Staudinger, M., Kauzlaric, M., Chardon, J., Favre, A. C., Hingray, B., Nicolet, G., Raynaud, D., Seibert, J., Weingartner, R., & Whealton, C. (2022). Comprehensive space-time hydrometeorological simulations for estimating very rare floods at multiple sites in a large river basin. *Natural Hazards and Earth System Sciences*, 22(9), 2891–2920. https://doi.org/10.5194/nhess-22-2891-2022
- Vousdoukas, M. I., Athanasiou, P., Giardino, A., Mentaschi, L., Stocchino, A., Kopp, R. E., Menéndez, P., Beck, M. W., Ranasinghe, R., & Feyen, L. (2023). Small Island Developing States under threat by rising seas even in a 1.5 °C warming world. *Nature Sustainability*, 6(12), 1552–1564. https://doi.org/10.1038/s41893-023-01230-5
- Vousdoukas, M. I., Mentaschi, L., Voukouvalas, E., Verlaan, M., Jevrejeva, S., Jackson, L. P., & Feyen, L. (2018). Global probabilistic projections of extreme sea levels show intensification of coastal flood hazard. *Nature Communications*, *9*(1), 2360. https://doi.org/10.1038/s41467-018-04692-w
  - Wahl, T., Jain, S., Bender, J., Meyers, S. D., & Luther, M. E. (2015). Increasing risk of compound flooding from storm surge and rainfall for major US cities. *Nature Climate Change*, 5(12), 1093–1097. https://doi.org/10.1038/nclimate2736
- Weibull, W. (1939). A statistical theory of strength of materials. Ing. Vetensk. Akad. Handl.
  - Wing, O. E. J., Bates, P. D., Sampson, C. C., Smith, A. M., Johnson, K. A., & Erickson, T. A. (2017). Validation of a 30 m resolution flood hazard model of the conterminous United States. *Water Resources Research*, *53*(9), 7968–7986. https://doi.org/10.1002/2017WR020917





970



- Wing, O. E. J., Lehman, W., Bates, P. D., Sampson, C. C., Quinn, N., Smith, A. M., Neal, J. C., Porter, J. R., & Kousky, C. (2022). Inequitable patterns of US flood risk in the Anthropocene. *Nature Climate Change*, 12(2), 156–162. https://doi.org/10.1038/s41558-021-01265-6
  - Yang, Z., García-medina, G., Wu, W., Wang, T., Leung, L. R., Castrucci, L., & Mauger, G. (2019). Estuarine, Coastal and Shelf Science Modeling analysis of the swell and wind-sea climate in the Salish Sea. *Estuarine, Coastal and Shelf Science*, 224(February), 289–300. https://doi.org/10.1016/j.ecss.2019.04.043
  - Yang, Z., Wang, T., Castrucci, L., & Miller, I. (2020). Modeling assessment of storm surge in the Salish Sea. *Estuarine, Coastal and Shelf Science*, 238(May 2019), 106552. https://doi.org/10.1016/j.ecss.2019.106552